Contrib Mineral Petrol (2005) 149: 647–665
DOI 10.1007/s00410-005-0672-9

ORIGINAL PAPER

Dmitri A. Ionov · Vladimir S. Prikhodko
Jean-Louis Bodinier · Alexander V. Sobolev
Dominique Weis

Lithospheric mantle beneath the south-eastern Siberian craton: petrology of peridotite xenoliths in basalts from the Tokinsky Stanovik

Received: 10 December 2004 / Accepted: 24 March 2005 / Published online: 31 May 2005

Abstract We provide petrographic, major and trace element data for over 30 spinel peridotite xenoliths from the Tokinsky Stanovik (Tok) volcanic field on the Aldan shield to characterize the lithospheric mantle beneath the south-eastern margin of the Siberian craton, which formed in the Mesoproterozoic. High equilibration temperatures (870–1,010°C) of the xenoliths and the absence of garnet-bearing peridotites indicate a much thinner lithosphere than in the central craton. Most common among the xenoliths are clinopyroxene-poor lherzolites and harzburgites with Al_2O_3 and CaO contents nearly as low as in refractory xenoliths from kimberlite pipes (Mir, Udachnaya) in the central and northern Siberian craton. By contrast, the Tok peridotites have higher FeO, lower Mg-numbers and lower modal orthopyroxene and are apparently formed by shallow partial melting ($\leq$ 3 GPa). Nearly all Tok xenoliths yield petrographic and chemical evidence for metasomatism: accessory phlogopite, amphibole, phosphates, feldspar and Ti-rich oxides, very high Na_2O (2–3.1%) in clinopyroxene, LREE enrichments in whole-rocks.

Keywords Siberian craton · Lithospheric mantle · Peridotite · Partial melting · Metasomatism

Electronic Supplementary Material Supplementary material is available for this article at http://dx.doi.org/10.1007/s00410-005-0672-9

Communicated by J. Hoefs

D. A. Ionov (✉) · A. V. Sobolev
Abteilung Geochemie, Max-Planck-Institut für Chemie,
Postfach 3060, 55020 Mainz, Germany
E-mail: ionov@mpch-mainz.mpg.de

D. A. Ionov · J.-L. Bodinier
Laboratoire de Tectonophysique (UMR 5568 CNRS),
ISTEEM, Université Montpellier 2, case 049,
34095 Montpellier cedex 05, France

D. A. Ionov · D. Weis
Department of Earth and Environmental Sciences,
Université Libre de Bruxelles CP160/02,
1050 Brussels, Belgium

V. S. Prikhodko
ITIG, Russian Academy of Sciences,
680063 Khabarovsk, Russia

D. Weis
E.O.S. University of British Columbia,
Vancouver, BC, Canada, V6T 1Z4

Introduction

The composition of the continental lithospheric mantle (CLM) beneath the Siberian craton remains poorly studied compared to the cratons in South Africa and North America, even though some of the first data on the cratonic CLM were obtained on xenoliths from Yakutian kimberlites (Sobolev 1977). Nearly all published petrological data for the CLM of the Siberian craton have been obtained on xenoliths from a small number of kimberlite pipes (Udachnaya, Mir and Obnazhennaya) located in its central and north-eastern parts known as the Anabar block (Fig. 1a). Those xenolith suites may not be representative of the CLM beneath the whole craton. Information on the CLM in the southern and western parts of the Siberian craton (Angara and Aldan-Stanovoy blocks; Fig. 1a) is very scarce. Studies of mantle samples from those areas are essential to better constrain the CLM compositions in Siberia.

It has long been known that volcanic rocks in the Tokinsky Stanovik range near the south-eastern rim of the Aldan shield (Fig. 1a) contain mantle xenoliths of the 'Cr-diopside' and 'Al-augite' series (Kiselev et al. 1979; Semenova et al. 1984). The site (referred to as 'Tok' below) is probably the only known occurrence of mantle xenoliths in Cenozoic basalts on the Siberian craton. Other basalt-hosted xenolith sites in southern Siberia are situated south of the craton rim (Kiselev et al. 1979; Ionov et al. 2005; Fig. 1a). Previous Russian studies (Kogarko et al. 1990; Semenova et al. 1984;

Solovyeva et al. 1988) defined several petrographic rock types among xenoliths from Tok and provided fragmentary whole-rock and mineral chemical data (the quality of which is hard to assess). To the best of our knowledge, no geochemical data on those xenoliths have been published as yet in peer-reviewed international literature.

This study provides petrographic descriptions, major and trace element whole-rock analyses and electron microprobe data for over 30 peridotite xenoliths from Tok (collected mainly in 1995 by the first two authors), which form the most extensive set of such data for basalt-hosted xenolith suites from southern Siberia. The large and fresh mantle xenoliths from Tok provide an excellent material for petrographic and whole-rock chemical studies, particularly when compared to the usually strongly altered xenoliths from the Yakutian kimberlites. The objectives of this work are: (1) characterize petrography, modal and chemical composition of the CLM beneath the SE margin of the Siberian craton. (2) Compare the Tok CLM with the CLM in other parts of the craton and in the nearby mobile belts. (3) Identify and characterize mantle depletion and enrichment events and establish their role in the origin and evolution of the CLM in the region. We show that the CLM beneath the SE Siberian craton is largely made up of highly refractory rocks, like in the central and north-eastern craton, but the partial melting in the Tok mantle took place at lower pressures. High temperatures in the shallow Tok CLM indicate a much higher geothermal gradient and thinner lithosphere than in the centre of the craton.

Geologic setting

The Aldan shield (Fig. 1a) is the largest area of exposed Archean and Paleoproterozoic crustal rocks on the Siberian platform (Zonenshain et al. 1990). The shield is made up of two blocks, the Aldan in the north and the Stanovoy in the south, separated by the Stanovoy suture zone. These two blocks are further divided into several granite-greenstone and granulite-gneiss terrains with ages from 1.9 Ga to 3.6 Ga (Frost et al. 1998; Jahn et al. 1998; Nutman et al. 1992). These terrains appear to have been amalgamated in a regional mid-Proterozoic (1.9–2.0 Ga) metamorphic event accompanied by widespread magmatism in the Stanovoy block.

Currently, the Aldan shield is un uplifted, seismically active area (Parfenov et al. 1987). The Stanovoy Range (Stanovik) mainly follows the Stanovoy suture zone, with outcrops of Early Proterozoic core metamorphic complexes and gabbro-anorthosite massifs (Gusev and Khain 1995). An area in the eastern Stanovoy Range, between Lake Toko on its northern slope and upper river Tok (a tributary of Zeya) on its southern slope, is usually called Tokinsky Stanovik, with summits reaching 2,000–2,400 m. Cenozoic alkali basaltic rocks (hawaiites, basanites, nephelinites) cover ~210 km^2 in this watershed region between the Lena and Amur river systems, mainly on its southern slope (Rasskazov et al. 2000; Semenova et al. 1984).

The xenoliths for this study were collected in lavas along the lower Nakit Creek near its confluence with the Tok river (Fig. 1b). Geographic coordinates (determined using GPS) are: 55°38′38″N, 130°06′09″E for the northernmost sampling site (9501) and 55°38′23″N, 130°05′53″E for the southernmost site (9506). Polyakov and Bagdasaryan (1986) reported a K–Ar age of 1.1 Ma for a basanite from the same locality and a range of 2.1–3.8 Ma for other volcanic rocks in the area. Rasskazov et al. (2000) obtained a much more narrow age interval (0.59–0.28 Ma) for volcanic rocks from the Tok site using laser Ar–Ar technique.

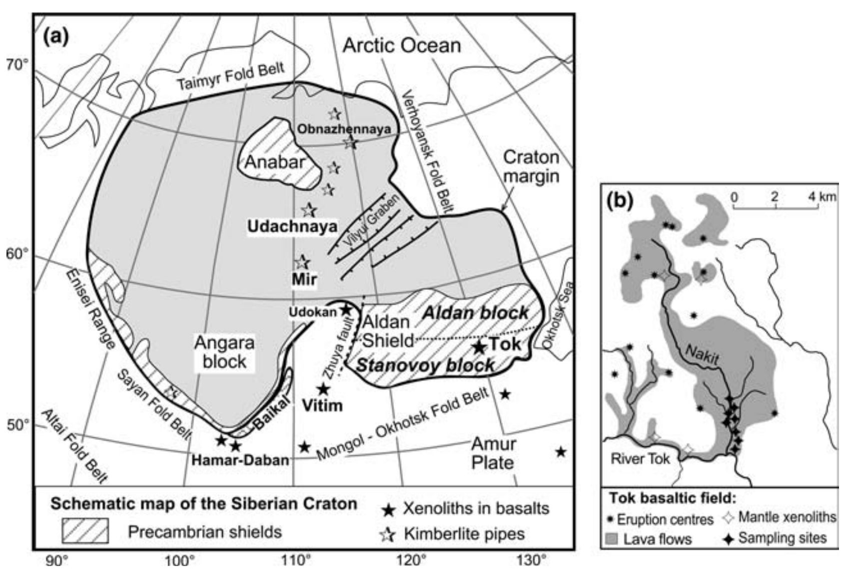

Fig. 1 a A sketch map of the Siberian craton and adjacent regions (modified from Zonenshain et al. 1990). **b** basaltic fields and mantle xenolith occurrences, upper river Tok

Sample preparation and analytical procedures

Most of the xenoliths were found among or inside massive lava blocks (Fig. 2a, b) produced mainly by the splitting of basalt by frost action on steep slopes of the creek canyon. Both xenoliths and host lavas show little effects of surface alteration, probably because of low summer rainfall and subzero temperatures for the most part of the year. Samples for this study were selected from a larger collection mainly based on their size (Fig. 2b), lack of alteration and basaltic veins. Our main purpose was to provide the best samples for chemical studies in terms of their freshness, homogeneity and size, in particular to obtain representative whole-rock powders. We concur with Boyd et al. (1997) that reliable estimates of mantle compositions require bulk analysis of large xenolith specimens because of common coarse grain size and locally irregular mineral distribution. The weight of the whole-rock samples is given in Table 1, which provides a summary of petrographic features, modal compositions and geothermometry.

We also made sure to select xenoliths from all eight sites at lower Nakit Creek (Fig. 1b) where they were found. It turned out later that the relative abundances of rock types at those sites may be different (e.g. most specimens collected in nearby sites 9505 and 9506 are lherzolites, while nearly all samples from site 9510 are harzburgites, Table 1). Thus, the choice of xenoliths from many outcrops helped to limit the effects of selective 'sampling' of mantle wall-rock by different batches of rising magma. Before our fieldwork at Tok, peridotite xenoliths from that area had been collected and crushed on-site to extract gem-quality olivine. It is likely that the mining activities preferentially consumed xenoliths with largest olivine (harzburgites) and left behind fine-grained and olivine-poor rocks.

The xenoliths were crushed, split and ground at Brussels University. Clean rock chips or slabs cut from central parts of xenoliths were crushed between two hydraulically driven wear-resistant tungsten carbide (WC) plates to $\leq$ 1–2 mm. The nearly new plates were inspected for signs of damage before and after crushing. The procedure yielded material free of metal chips (common in samples crushed in steel mortars). Cross-contamination was negligible because the device is easy to clean. The weight of the crushed rocks ranged from 140 g to 1,100 g (usually $>$200 g, Table 1), which appeared to provide a representative whole-rock sample of each xenolith considering its grain size, texture and homogeneity. Split aliquots of the crushed material were ground to a fine powder in agate jars using either a shatter-box (40–60 g of powder) or a planetary mill (90–120 g). Another aliquot of the crushed rock was sieved. Clean mineral grains were hand-picked from appropriate size fractions (usually 0.5–1 mm), mounted on round 25 mm epoxy disks and polished for micro-beam analyses.

The contents of major oxides in 29 peridotites were determined by wavelength-dispersive X-ray fluorescence (XRF) spectrometry at the University of Niigata (Japan) using low-dilution (5:1) fused beads. The technique (Takazawa et al. 2003) was designed to make high-precision analyses of peridotites including elements at low abundances (K, Na, P, Ni, Cr, Ca, Al). The rock powders were weighed and ignited in platinum beakers for ≥6 h at 900°C. The procedure turned all FeO into Fe_2O_3 and expelled water and CO_2. All the samples gained weight due to Fe^{2+} oxidation indicating low volatile contents and hence low alteration degrees. The ignited powders were fused with lithium tetraborate and $LiBO_2$ to produce beads, which were analysed using ultramafic reference rock samples as external standards. Four duplicates and three other xenoliths were analysed by a similar XRF method, at Mainz University, on fused beads (7:1 dilution) made using ignited powders (Ionov et al. 2005). The match between the Mainz and Niigata data is excellent for the first batch of Niigata analyses (sites 9506 to 9510; Table 2). SiO_2 and MgO values as well as the totals from the second batch of Niigata analyses (9501 to 9505) are somewhat low, probably due to the use of a different batch of lithium borates.

Fig. 2 **a** Xenolith-bearing massive lavas near the Nakit Creek. **b** Xenolith 9508-10 (*outlined in white*) and its host lava. All xenoliths from this study were found in massive lavas

Table 1 A summary of petrographic and modal data and temperature estimates

Sample number	WR (g)	Rock type	Mg# Ol	Black vugs	Fluid inclusions	Calculated modal abundances (wt.%)							*T* (°C) Ca-Opx
						Ol	Opx	Cpx	Spl	Fs	Ap	Phl,Am	
9501-2	268	Harzburgite	0.913	+	–	78.6	17.2	3.1	0.3	0.7	0.12		910
9501-3	257	Harzburgite	0.912	+	–	80.1	13.4	5.0	0.3	1.1	0.09		907
9501-13	182	Harzburgite	0.910*	–	+	80.1	15.6	2.7	0.6	0.9	0.09	+	933
9502-6	320	Low-Cpx lh.	0.899*	–	+ +	67.4	25.4	5.6	0.6	0.9	0.09		980
9502-9	316	Harzburgite	0.914	+	+	79.2	15.7	3.1	0.5	1.5	0.08		874
9503-4	139	Harzburgite	0.910*	+	–	73.7	20.9	3.3	0.7		0.06	1.4	910
9503-19	162	Low-Cpx lh.	0.900*			70.5	21.1	6.2	0.8	1.3	0.11		931
9505-3	184	Lherzolite	0.904	+	–	73.7	15.2	9.4	0.0	1.5	0.24		907
9506-0	154	Harzburgite	0.919			79.9	14.9	2.8	0.6	1.5	0.34		890
9506-1	1100	Lherzolite	0.895	–	–	54.6	25.8	17.0	2.5				1010
9506-2	398	Lherzolite	0.895	+ +	–	53.9	26.3	17.3	2.5				1001
9506-3	290	Lherzolite	0.909*	–	+	54.6	33.2	10.2	1.0	0.8	0.04		976
9507-1	780	Low-Cpx lh.	0.911	+	+	78.6	15.1	5.0	0.4	0.8	0.10		985
9507-5	340	Lherzolite	0.901	+	–	57.2	26.5	14.2	2.1				985
9508-1	629	Low-Cpx lh.	0.904*	+	+	73.6	17.5	6.7	1.0	1.3	0.07	(phl?)	1005
9508-2	780	Low-Cpx lh.	0.906	+	+ +	74.1	18.8	5.8	0.7	0.6	0.11		976
9508-3	458	Harzburgite	0.903*	+	+ +	73.5	20.3	4.1	0.5	1.5	0.11	(phl?)	956
9508-5	885	Lherzolite	0.901*	+	+	63.4	24.1	10.5	1.6	0.4	0.06	0.5	1004
9508-6	≥600	Lherzolite	0.896*	+	–	59.4	22.5	15.1	2.3	0.6			985
9508-7	567	Harzburgite	0.911	+	+ +	76.8	16.7	4.8	0.5	1.1	0.12	(am?)	968
9508-8	719	Harzburgite	0.911*	+	+	72.0	22.7	3.7	0.6	1.0	0.08	(am?)	955
9508-11	833	Harzburgite	0.913	+	+	77.6	17.5	4.5	0.4		0.08		957
9508-31	256	Harzburgite	0.916	+ +	–	76.5	16.6	4.8	0.4	1.7	0.06		887
9508-39	180	Lherzolite	0.894	+	+	53.9	26.3	17.2	2.6				964
9508-40	150	Harzburgite	0.913	+	–	71.3	24.0	3.7	0.5		0.41	(am?)	922
9508-50	347	Harzburgite	0.912	–	–	77.1	17.6	3.6	0.7	0.9	0.07		992
9510-2	464	Harzburgite	0.915	+ +	–	77.2	16.6	4.3	0.4	1.3	0.12		914
9510-4	400	Harzburgite	0.914	+	–	79.9	16.0	2.7	0.4	1.0	0.11		926
9510-8	235	Harzburgite	0.908	+	+	79.2	14.9	4.9	0.4	0.6	0.08		950
9510-16	235	Low-Cpx lh.	0.899*	+	–	76.2	17.4	6.0	0.4				957
9510-17	217	Harzburgite	0.907	+	+	75.6	19.5	3.6	1.3				1011
9510-19	222	Harzburgite	0.911	–	–	72.7	22.8	3.4	0.7		0.30		951

Ol olivine; *Opx* orthopyroxene, *Cpx* clinopyroxene, *Spl* spinel, *Fs* feldspar; *Phl* phlogopite; *Am* amphibole. Petrographic features: – absent; + present; + + abundant; (am, phl), minerals replaced by fine-grained Fs-bearing material. Mg#, $Mg/(Mg+Fe)_{at}$; values with asterisk (*) are for heterogeneous olivine (1σ/mean > 1% for FeO and > 0.1% for MgO; see Table 1 of ESM). *WR*, weight of crushed whole-rock samples. *T* estimates are after Brey and Kohler (1990). Modal apatite (Ap) was calculated for xenoliths with ≥0.03% P_2O_5

Minerals were studied by electron probe microbeam analysis (EPMA) at the Service Microsonde Sud (Université Montpellier 2) and Université Blaise Pascale, Clermont-Ferrand on Cameca SX-100 instruments with routine conditions: 20 kV voltage, 10 nA current, 20–30 s counting times. Standards were natural minerals, synthetic oxides and pure metal. Concentrations were obtained from raw intensities using 'X-PHI' (Merlet 1994) method at Montpellier and PAP at Clermont-Ferrand. Major minerals were first analysed in grain mounts; selected samples were analysed in thin sections to study accessory phases and mineral zoning in major minerals. High-precision olivine analyses were obtained with a Jeol JXA8200 instrument at Max-Planck-Institut für Chemie (Mainz) using 20 kV accelerating voltage, 20 nA current and extended counting times (120 s) for Ca, Al, Cr, Ni, Mn and Fe. Calibration was done on wollastonite (Ca), San Carlos olivine (USNM 111312/444; Jarosewich et al. 1980) (Si, Mg, Fe), rodonite (Mn) and oxides; ZAF correction was applied. The San Carlos olivine was also measured together with Tok olivines to yield a repeatability of 0.2% (1σ) for Mg, 0.4% for Fe, 1.2% for Ni, 4% for Mn and Ca, and 0.03% for Mg/(Mg + Fe) (25 analyses). Modal compositions were calculated from whole-rock and mineral analyses by mass balance using least-squares regression.

Whole-rock xenoliths were analysed for trace elements by solution inductively coupled plasma mass-spectrometry (ICPMS). Rock powders (~100 mg) were digested with HF–HNO_3–$HClO_4$ mixtures, evaporated with small amounts of $HClO_4$ and 6 N HNO_3 and made up to 100 ml with 1% HNO_3. Five samples were processed at clean laboratory facilities at Brussels and analysed on a VG Elemental Plasma Quad II ICPMS instrument at the European Geochemical Facility at Bristol University, UK using multi-element synthetic standards for external calibration and internal standards for drift correction. Another five xenoliths and host basalt were analysed on a similar instrument at Montpellier following routine techniques established at that laboratory (Ionov et al. 1992b; Kalfoun et al. 2002). Two sets of composite synthetic standards were used for calibration; samples were spiked with In and Bi for drift correction. Synthetic solutions were used to correct for

Table 2 XRF analyses of whole-rock samples

Sample number	SiO_2	TiO_2	Al_2O_3	Cr_2O_3	FeO	MnO	NiO	MgO	CaO	Na_2O	K_2O	P_2O_5	Total	CMI (%)	Mg#	CaO/Al_2O_3
Peridotite xenoliths of the lherzolite–harzburgite series (Mg#≥0.89)																
9501-2	43.72	0.006	0.63	0.33	7.89	0.127	0.329	45.47	0.72	0.14	0.03	0.06	99.5	0.4	0.911	1.15
9501-3	43.50	0.034	0.70	0.38	8.02	0.132	0.315	45.14	1.04	0.18	0.07	0.05	99.6	0.4	0.909	1.50
9501-13	43.06	0.032	0.86	0.38	8.20	0.130	0.323	45.29	0.72	0.09	0.02	0.04	99.2	0.4	0.908	0.84
9501-13[a]	43.57	0.036	0.88	0.40	8.03	0.132	0.331	45.75	0.70	0.09	0.02	0.04	100.0	0.4	0.910	0.79
9502-6	44.61	0.052	1.25	0.40	9.38	0.146	0.270	41.58	1.35	0.16	0.06	0.04	99.3	0.5	0.888	1.08
9502-9	43.30	0.030	0.74	0.36	7.91	0.125	0.319	45.27	0.74	0.12	0.07	0.03	99.0	0.4	0.911	0.99
9502-9[a]	44.02	0.035	0.76	0.39	7.76	0.123	0.324	45.78	0.72	0.11	0.07	0.03	100.1	0.4	0.913	0.95
9503-4	43.29	0.038	1.10	0.35	8.31	0.138	0.302	43.86	0.78	0.15	0.09	0.03	98.5	0.4	0.904	0.71
9503-19[a]	44.38	0.065	1.30	0.38	8.57	0.154	0.284	42.74	1.47	0.17	0.04	0.05	99.6	0.2	0.899	1.13
9505-3	44.08	0.013	1.25	0.35	8.34	0.132	0.287	42.53	2.01	0.25	0.03	0.11	99.4	0.4	0.901	1.60
9506-0[a]	43.85	0.016	0.79	0.40	7.32	0.123	0.313	46.31	0.81	0.12	0.08	0.16	100.3	0.3	0.919	1.03
9506-1	45.07	0.162	3.94	0.33	8.32	0.137	0.236	38.02	3.55	0.33	0.01	0.02	100.1	0.3	0.891	0.90
9506-2	45.14	0.163	3.98	0.33	8.27	0.137	0.233	37.89	3.62	0.35	0.02	0.02	100.1	0.3	0.891	0.91
9506-3	46.62	0.048	2.42	0.38	7.39	0.131	0.254	40.31	2.41	0.24	0.04	0.02	100.2	0.2	0.907	0.99
9506-3[a]	46.71	0.053	2.47	0.41	7.33	0.129	0.263	39.98	2.36	0.21	0.03	0.02	100.0	0.3	0.907	0.96
9507-1	43.72	0.040	0.82	0.39	8.09	0.131	0.313	45.19	1.14	0.16	0.03	0.05	100.1	0.4	0.909	1.40
9507-5	45.10	0.103	3.34	0.37	8.01	0.134	0.244	39.50	3.08	0.27	0.02	0.01	100.2	0.3	0.898	0.92
9508-1	43.89	0.057	1.64	0.38	8.39	0.133	0.288	43.45	1.58	0.18	0.07	0.03	100.1	0.4	0.902	0.96
9508-2	44.18	0.016	1.26	0.37	8.23	0.131	0.297	43.99	1.31	0.17	0.03	0.05	100.0	0.4	0.905	1.04
9508-3	44.32	0.073	1.14	0.39	8.69	0.142	0.298	43.82	1.05	0.16	0.09	0.05	100.2	0.4	0.900	0.93
9508-5	44.48	0.088	2.60	0.35	8.26	0.135	0.268	41.23	2.27	0.24	0.03	0.03	100.0	0.4	0.899	0.87
9508-6	44.70	0.140	3.58	0.36	8.35	0.136	0.245	38.92	3.20	0.35	0.03	0.02	100.0	0.4	0.893	0.90
9508-7	44.03	0.032	0.91	0.43	7.95	0.128	0.300	44.86	1.12	0.16	0.08	0.06	100.1	0.4	0.910	1.23
9508-8	44.63	0.063	1.08	0.39	8.41	0.137	0.294	44.00	0.93	0.13	0.06	0.04	100.2	0.4	0.903	0.86
9508-11	43.96	0.031	0.75	0.37	7.91	0.131	0.315	45.59	1.01	0.13	0.03	0.04	100.3	0.2	0.911	1.35
9508-31	44.26	0.021	1.02	0.37	7.45	0.130	0.308	45.10	1.07	0.25	0.07	0.08	100.1	0.3	0.915	1.04
9508-31[a]	44.28	0.030	1.11	0.40	7.40	0.131	0.310	44.95	1.01	0.18	0.07	0.07	99.9	0.2	0.915	0.91
9508-39	44.99	0.162	3.92	0.35	8.29	0.137	0.236	37.75	3.60	0.37	0.05	0.03	99.9	0.3	0.890	0.92
9508-40[a]	43.91	0.030	0.86	0.43	7.68	0.121	0.318	45.10	1.00	0.12	0.07	0.16	99.8	0.3	0.913	1.16
9508-50	43.81	0.047	1.14	0.38	8.06	0.127	0.313	45.36	0.96	0.10	0.03	0.04	100.4	0.4	0.909	0.85
9510-2	44.09	0.041	0.80	0.41	7.60	0.133	0.310	45.66	0.96	0.24	0.05	0.06	100.3	0.4	0.915	1.21
9510-4	43.76	0.024	0.77	0.36	7.92	0.132	0.326	45.96	0.65	0.16	0.05	0.05	100.2	0.4	0.912	0.85
9510-8	43.45	0.027	0.79	0.38	8.39	0.132	0.310	45.13	1.02	0.19	0.03	0.04	99.9	0.4	0.906	1.29
9510-16	43.86	0.045	0.90	0.38	8.96	0.137	0.296	44.09	1.19	0.20	0.02	0.02	100.1	0.4	0.898	1.32
9510-17	43.31	0.054	1.64	0.38	8.45	0.131	0.294	44.64	0.92	0.11	0.02	0.02	100.0	0.5	0.904	0.56
9510-19	44.28	0.025	0.89	0.41	7.86	0.130	0.307	44.86	1.07	0.11	0.01	0.14	100.1	0.3	0.910	1.20
Reference sample (harzburgite JP-1)																
JP-1[a] av3	43.78	0.012	0.72	0.43	7.62	0.121	0.326	45.95	0.56	0.02	0.00	0.01	99.5	−2.4	0.915	
JP-1 RV	43.74	0.00	0.64	0.45	7.75	0.12	0.323	46.14	0.58	0.02	0.00	0.00	99.8		0.914	
Host basalt																
9508-1b[b]	45.22	2.37	14.69	0.03	9.74	0.17	0.05	9.38	8.46	4.57	3.37	1.09	99.7		0.632	0.6

CMI change of mass on ignition (positive values indicate overall weight gain due to oxidation of FeO to Fe_2O_3). JP-1 data is an average of three replicate analyses done together with the xenoliths, *RV* recommended values

[a]Analysed at Mainz

[b]Analysis from Ionov et al. (2005). Mg#, $Mg/(Mg+Fe)_{at}$

oxide interference. Reference samples BEN, BHVO-1, BHVO-2, BIR-1, JP-1, PCC-1were analysed and used as unknowns for quality control.

Petrography

Xenoliths from the lower Nakit Creek (Fig. 1b) can be grouped as (1) 'green' spinel (Spl) peridotites and (2) clinopyroxene–olivine (Cpx–Ol) cumulates and rare pyroxenites. We further identify two rock series among the non-cumulate peridotites based on microstructures, mineral proportions (Streckeisen 1976) and Mg-numbers Mg#, $Mg/(Mg+Fe)_{at}$: lherzolite–harzburgite (LH) and lherzolite–wehrlite (LW). The LH series groups 'normal' (in terms of pyroxene abundances and Mg#) spinel peridotites, which can be considered residues of melt extraction from a fertile source (Fig. 3a–d). The LW series is characterized by complete or large-scale replacement of orthopyroxene (Opx) by Cpx and low Mg# (≤ 0.88). This study only concerns the LH series rocks, which are by far the most abundant (≥70–80% of collected xenoliths).

The great majority of the xenoliths in this study are rich in olivine (70–80%) and poor in Cpx (3–7%) (Table 1, Fig. 4). Out of 32 rocks, for which modal data are available, 18 are harzburgites (≤ 5% Cpx) followed by Cpx-poor (5–7%) lherzolites; only five are fertile lherzolites (55–59% Ol, 14–17% Cpx). Moreover, the olivine-rich xenoliths may have been preferentially scavenged at the site by mining (see Sample preparation and analytical procedures). In any case, the refractory peridotites are clearly the dominant rock types in the LH series.

Fertile lherzolites are coarse- to medium-grained and have protogranular microstructures (Harte 1977) with common irregularly shaped, large spinel grains (Fig. 3a). Pyroxenes and spinel in unmetasomatized Cpx-poor peridotites usually have smaller grain size and more equant shapes with regular (curvilinear or straight) boundaries (Fig. 3b). Many harzburgites have very large (5–10 mm) olivine grains with preferred linear orientation (Fig. 3d). Some Cpx-poor peridotites contain clusters of olivine neoblasts cross-cutting the coarse olivine (Fig. 3c).

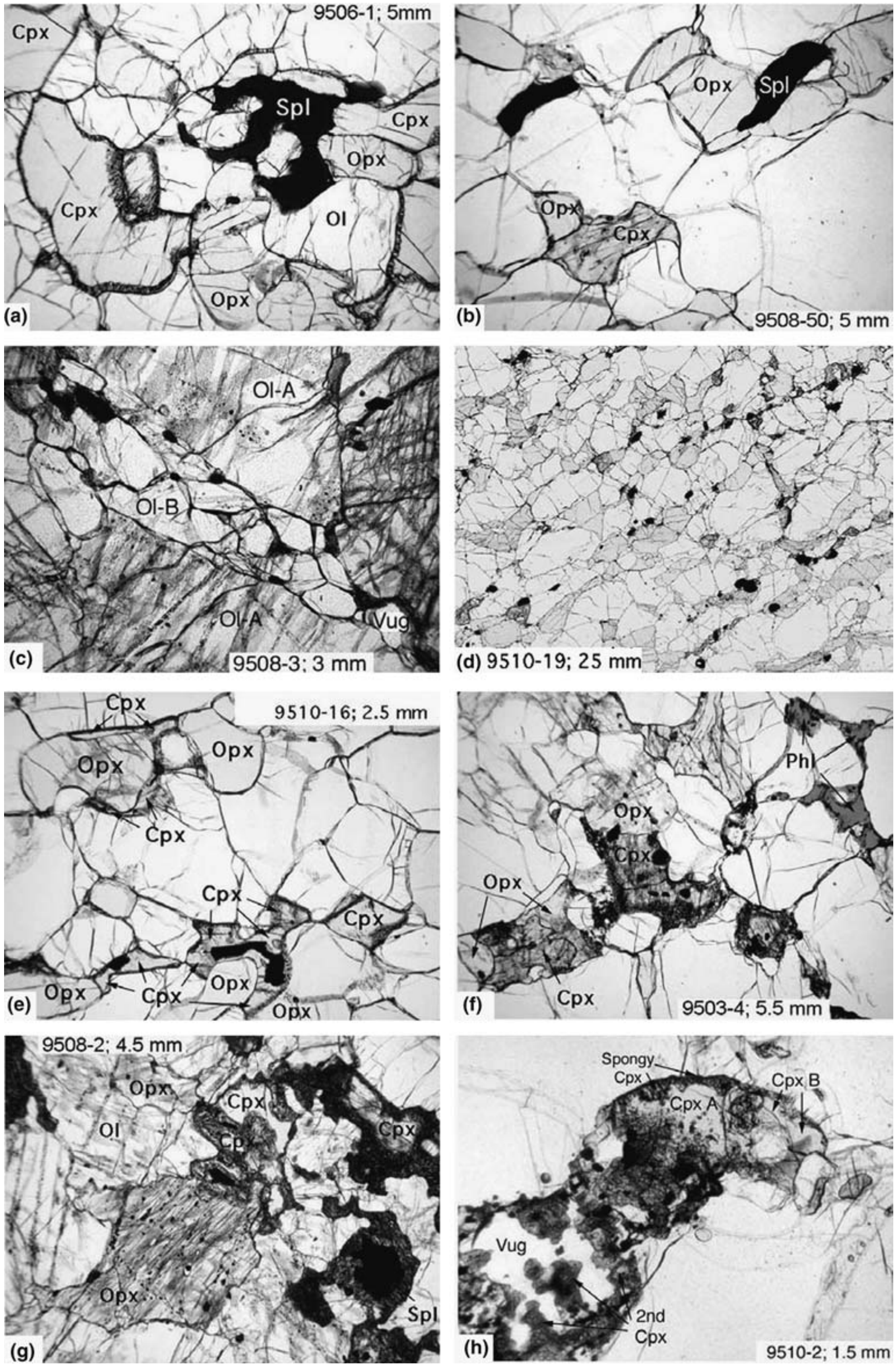

Fig. 3 Photomicrographs of the lherzolite–harzburgite (LH) series xenoliths from Tok in plane-polarized transmitted light. Sample numbers and the horizontal field of view are given on the photographs. *Ol* olivine, *Opx* orthopyroxene, *Cpx* clinopyroxene, *Spl* spinel. **a** Fertile spinel lherzolite (17% Cpx). **b** Spinel harzburgite (4% Cpx) without metasomatic phases. **c** Coarse, fractured olivine (Ol-A) and subhedral olivine neoblasts (Ol-B) in a harzburgite. The neoblasts are associated with small vugs and pockets of opaque material. **d** Preferred linear orientation of large olivine grains, clusters of small Spl and Cpx–Spl aggregates. **e** Cpx develops around spinel and partially replaces Opx to form Cpx-Spl clusters in a low-Cpx (6%) lherzolite. **f** Interstitial phlogopite (Phl) and metasomatic Cpx in a harzburgite. Opx is locally replaced by Cpx. Pyroxene grains contain cloudy domains with fluid micro-inclusions; many Cpx grains have spongy rims. **g** Metasomatic Cpx (note spongy rims) and abundant fluid inclusions in Cpx-poor (6%) lherzolite. **h** Metasomatic cavities (vugs) and two generations of clear Cpx (with different chemical compositions; Table 3) in a harzburgite. Late-stage Cpx (with abundant vermicular micro-channels and inclusions) replaces Cpx-A and Cpx-B. The vugs are empty and contain no silicate glass; their walls are lined with fine-grained second-generation Cpx, olivine and black Cr-rich spinel

Petrographic evidence for metasomatism is rare in the fertile lherzolites but very common in olivine-rich peridotites (Fig. 3e–h). Some xenoliths contain accessory volatile-bearing minerals: phlogopite, amphibole and apatite (Table 1). Phlogopite forms anhedral interstitial (Fig. 3f) or subhedral prismatic grains sometimes grouped in clusters. In many cases, phlogopite and amphibole are completely or partially replaced by fine-grained aggregates of alkali feldspar, oxide minerals and second-generation olivine, Cpx and spinel. Such aggregates preserve the shapes and cleavage cracks of the pre-existing minerals; the second-generation olivine grains are elongated and parallel to the pre-existing cleavage. Similar aggregates were found in other xenolith suites from southern Siberia (Ionov et al. 1995b, 1999). In addition to apatite, some Tok xenoliths also contain whitlockite, a (Na,Mg)-bearing, volatile-free phosphate, which is common in extraterrestrial rocks, but has not been earlier found in the earth's mantle. The presence of whitlockite was confirmed by Raman micro-spectroscopy at Mainz University.

Metasomatic Cpx can be recognized in many olivine-rich peridotites. Most commonly, it replaces Opx grains along boundaries (Fig. 3e) or inside (Fig. 3f). Cpx may also enclose spinel (Fig. 3e) to form elongated aggregates and clusters, which follow preferred linear orientation of coarse olivine (Fig. 3d). In some samples, two generations of clear and fairly large Cpx grains can be identified by textural position, colour and/or EPMA data (Cpx-A and Cpx-B in Fig. 3h).

Many Tok xenoliths also contain a distinct textural type of Cpx, which either makes up spongy aggregates with abundant vermicular micro-channels replacing the coarse and clear Cpx (Fig. 3f, g) or is a major component in interstitial material (Fig. 3h). The textural evidence clearly indicates that the fine-grained Cpx is secondary in the sense that it is formed by late-stage processes. Importantly, the secondary Cpx (as well as other interstitial materials) is not normally enclosed in silicate glass. Furthermore, it is not more common at the margins of Tok xenoliths than in their cores and is not spatially or texturally related to host basalt. We assume, therefore, that this second-generation Cpx (locally intergrown with second-generation Ol and Spl) formed in the mantle, possibly shortly before the transport of the xenoliths to the surface.

Further evidence for metasomatic additions of Cpx in the Tok xenoliths comes from comparisons of their modal compositions with those in other spinel peridotite suites. Some olivine-rich (> 72%) Tok samples have higher Cpx abundances than the Udachnaya xenoliths and peridotites from the Horoman massif in Japan (Fig. 4), possibly because of the formation of small amounts (≤ 2–3%, Fig. 4) of metasomatic Cpx in the Tok peridotites. Modal abundances in fertile Tok samples (which have no metasomatic Cpx) fall into the range for xenoliths from nearby off-craton sites in central Asia (Fig. 4).

Olivine and pyroxenes in many Tok xenoliths contain abundant fluid inclusions (Table 1; Fig. 3f, g). The smallest inclusions are most commonly CO_2-filled and locally form dense dark 'clouds' while larger (> 10 μm) ones are empty and tend to form arrays along grain margins or crack systems. Usually, Opx is the mineral with most abundant inclusions (Fig. 3g). Some micro-inclusions contain glass (i.e. are melt inclusions) or are composite, with glass, fluid and mineral components (V. Kamenetsky and P. Schiano, personal communications, 2000–2003).

An unusual feature of many Tok xenoliths (listed in Table 1) is the irregularly shaped and distributed empty cavities, whose walls are lined with second-generation

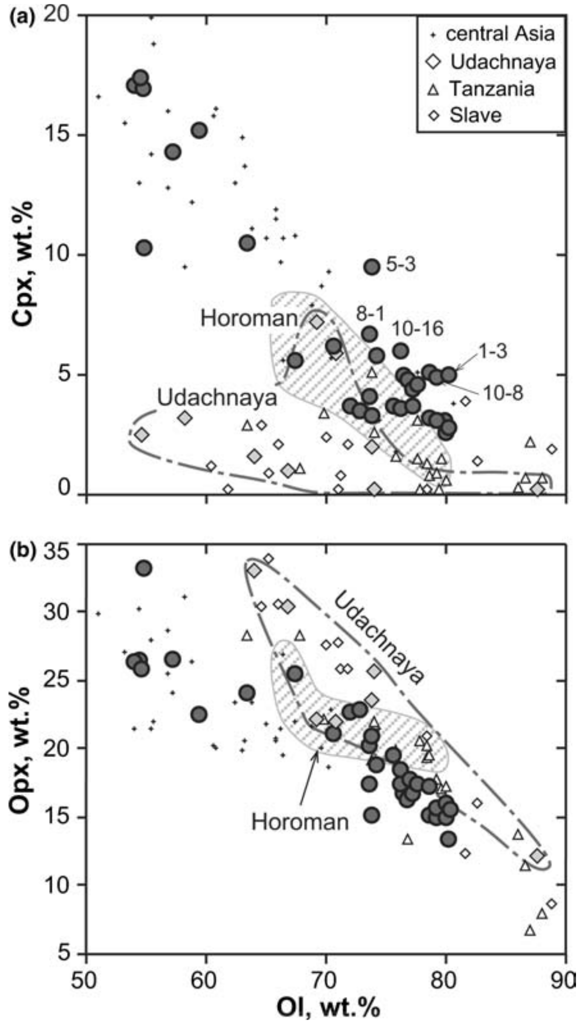

Fig. 4 Modal abundance co-variation plots for Tok LH series peridotites (*filled circles*): **a** Ol–Cpx, **b** Ol–Opx. Shown for comparison are spinel peridotite xenoliths from Udachnaya in central Siberian craton (Boyd et al. 1997), northern Slave (Kopylova and Russell 2000) and Tanzania (Lee and Rudnick 1999) cratons, basalt-borne xenoliths in southern Siberia and Mongolia (Ionov et al. 2005; Press et al. 1986; Wiechert et al. 1997) and the field (*grey diagonal pattern*) for feldspar-poor (< 2%) Horoman peridotites (Takazawa et al. 2000). Abbreviated numbers are shown for samples mentioned in the text

Ol, Cpx and Spl (Fig. 3h). The cavities range in size from tens of microns to several millimetres. The larger ones were originally recognized in hand specimens as "black holes" because of the abundant fine-grained black spinel inside. The cavities in the Tok xenoliths typically contain no silicate glass or its alteration products and hence are distinct from "melt pockets" or interstitial aggregates of glass with vugs that are common in many basalt-borne xenolith suites (Chazot et al. 1996; Francis 1987; Frey and Green 1974; Ionov et al. 1994; Wiechert et al. 1997). Another major difference is that the "black vugs" in the Tok xenoliths are not related to the breakdown of a specific mineral phase, like amphibole or Cpx (Frey and Green 1974; Ionov et al. 1994; Yaxley and Kamenetsky 1999).

Whole-rock major element compositions

Whole-rock XRF data are given in Table 2. The majority of the samples (24 out of total 32) have fairly uniform contents of MgO (43.5–46%), CaO and Al_2O_3 (0.6–1.3%). These refractory (Ol-rich, Cpx-poor) peridotites are strongly depleted in 'basaltic' components (Al, Ca, Ti) and rich in Mg and Ni relative to model primitive mantle (Palme and O'Neill 2003). Five Cpx-rich xenoliths can be characterized as fertile (MgO <40%; CaO, Al_2O_3 >3%). Moderately depleted rocks are rare; only two Tok samples have Al_2O_3 between 1.7% and 3.3% (Fig. 5a), while a large proportion of xenoliths in basalts worldwide have Al_2O_3 in that range (Pearson et al. 2003).

The variation ranges for Al_2O_3 (Fig. 5a), CaO, NiO (Fig. 6b) and Cr_2O_3 in the refractory Tok xenoliths are similar to those in peridotites from Udachnaya (Boyd et al. 1997) and other sites in central and north-eastern Siberian craton (Spetsius and Serenko 1990; Ukhanov et al. 1988). By contrast, the refractory Tok xenoliths have less broad ranges of SiO_2 and MgO and generally lower SiO_2 contents, consistent with a narrower modal Ol–Opx range and the absence of Opx-rich peridotites (Fig. 4b). Furthermore, the Tok xenoliths typically have higher FeO and MnO (Figs. 5b, 6d) and lower Mg# than coarse (low-*T* garnet and spinel) peridotites from Siberian and other kimberlites (Boyd et al. 1997; Pearson et al. 2003). The MgO and FeO contents and Mg# in the Tok xenoliths are similar to those in sheared, high-*T* garnet peridotites from Udachnaya (Fig. 5b) believed to be affected by melt metasomatism. By contrast, the Tok xenoliths have lower TiO_2 (Fig. 6a) and higher Na_2O (Fig. 6c) and P_2O_5.

The Tok peridotites plot in Figs. 5 and 6 mainly within the fields of xenoliths in basalt from nearby southern Siberia and Mongolia. However, the two data sets differ in relative abundances of fertile and refractory peridotites. The Tok suite is dominated by refractory rocks while moderately depleted peridotites are rare and very fertile (e.g. Al_2O_3 >4%) lherzolites are absent. By contrast, highly refractory rocks are rare among the generally fertile off-craton xenolith suites from central Asia (Ionov 2002; Ionov et al. 2005; Press et al. 1986).

Also plotted for comparison in Figs. 5 and 6 (as fields) are peridotites from the Horoman massif (situated close to Tok) because they were shown to closely match partial melting trends and are poorly affected by metasomatism (Takazawa et al. 2000). The Tok xenoliths typically plot within the fields for Horoman peridotites, except that the latter extend to slightly higher MgO but lower CaO and Al_2O_3 (Fig. 5a) contents. On the other hand, many refractory Tok xenoliths have higher FeO, MnO, TiO_2 and Na_2O than the Horoman rocks (Figs. 5b, 6). These differences as well as high K_2O (0.01–0.09%) and P_2O_5 (0.01–0.18%) in Tok xenoliths with accessory alkali feldspar and phosphates (Tables 1, 2) may be related to metasomatism in the Tok samples.

The contents of MgO in the Tok xenoliths are negatively correlated with Al_2O_3 (Fig. 5a), CaO, SiO_2, Na_2O and TiO_2 and positively correlated with NiO (Fig. 6). By contrast, the plots of MgO versus FeO (Fig. 5b) and MnO (Fig. 6d) do not define clear trends

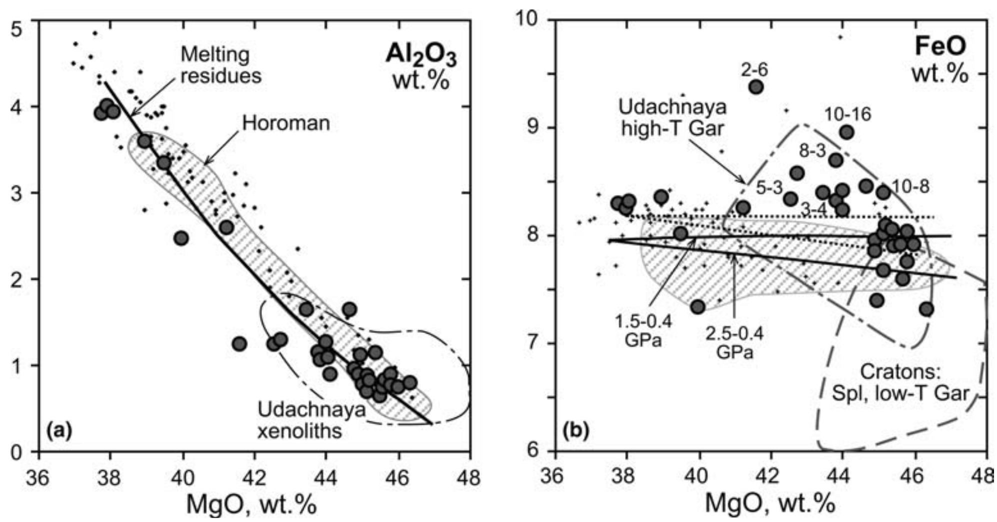

Fig. 5 Plots of MgO versus Al_2O_3 (**a**) and FeO (**b**) in LH series Tok xenoliths. *Solid black lines* show residues from polybaric (2.5–0.4 and 1.5–0.4 Ga) fractional melting of fertile spinel lherzolite (Niu 1997; Takazawa et al. 2000). *Dashed black lines* in (**b**) show batch partial melt extraction residues (0–25%) from fertile peridotite at 0.5 and 2 GPa (Walter 2003). Other symbols and data are as in Fig. 4

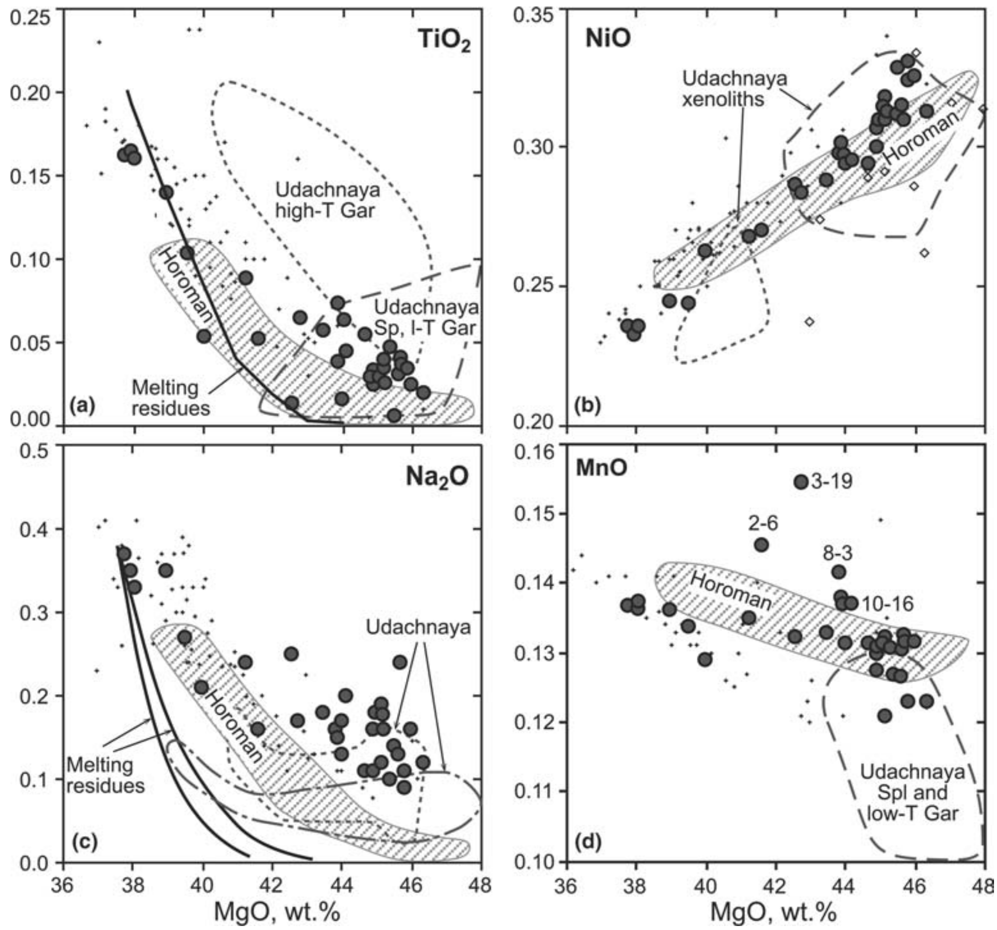

Fig. 6 Co-variation plots for MgO with minor oxides (wt.%). Symbols and data sources are as in Figs. 4 and 5

Fig. 7 Plots of Al_2O_3 vs. FeO (**a**) and Ca/Al (**b**) for LH series Tok xenoliths. *Dashed lines* in (**a**) show residues of batch melting at 1–3 GPa; *dotted lines* are for decompression fractional melting from 3 to 1 GPa (0–26%) and 5 to 1 GPa (0–38%) (Herzberg 2004). Other symbols and data sources are as in Fig. 4. *Lighter circles* show samples with heterogeneous olivine (1σ mean >1% for FeO and >0.1% for Mg# for averages of eight analyses; Table 1 of ESM) attributed to post-melting Fe-enrichment. High FeO and Ca/Al in the refractory rocks cannot be produced by partial melting and are inferred to be metasomatic

apparently because some rocks with intermediate MgO contents (41–45%) have relatively high FeO and MnO. Whole-rock Mg–Fe variations may be inter-dependent due to coupled Mg–Fe substitutions in olivine, pyroxenes and spinel; e.g. metasomatic Fe-enrichment in olivine decreases MgO in olivine and hence in bulk rock. A better insight into the behaviour of iron can be obtained by plotting it against Al, which is broadly considered as a robust partial melting index in mantle

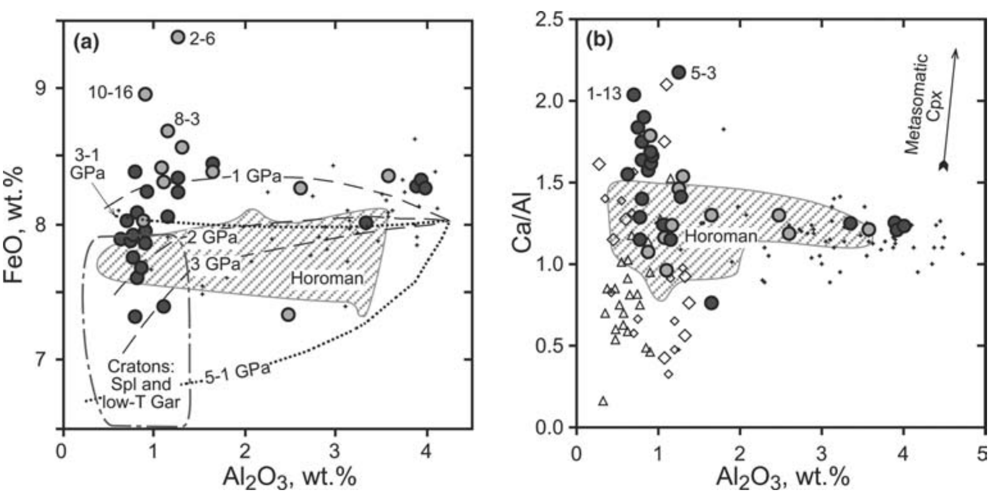

Table 3 EPMA data for second-generation and metasomatic minerals

	9502-6		9503-19		9508-40						9510-19		
	Ol-A av.4	Ol-B av.2	Ol-A	Ol-B	Ol-2nd av.2	Spl-L.	Spl-2nd av.2	Cpx-A	Cpx-B av.2	Cpx Spongy	Cpx-A av.3	Cpx-B av.2	Cpx-2nd av.2
SiO_2	40.76	40.80	40.86	40.63	39.96	0.13	0.42	52.98	51.22	53.17	54.21	53.89	53.62
TiO_2						0.13	1.38	0.11	0.12	0.09	0.18	0.12	0.16
Al_2O_3						22.56	31.70	4.90	3.39	1.81	4.26	2.95	2.84
Cr_2O_3					0.09	47.40	34.60	2.72	3.08	1.43	1.22	1.15	1.04
FeO	9.73	10.48	9.80	11.48	8.65	15.90	13.75	2.63	2.51	2.45	2.68	2.35	2.37
MnO	0.15	0.13	0.14	0.17	0.16	0.27	0.24	0.13	0.00	0.06	0.06	0.04	0.09
MgO	48.23	47.81	49.30	47.71	50.80	14.61	16.64	15.05	17.11	17.95	15.93	16.40	16.99
CaO	ND	ND	ND	ND	0.17			17.63	19.75	22.12	18.62	20.30	21.69
Na_2O								2.95	1.21	0.62	2.44	1.70	0.90
NiO	0.39	0.40	0.40	0.35	0.36	0.19	0.21	0.05	0.05	0.06			
Total	99.3	99.6	100.5	100.4	100.3	101.2	99.3	99.2	98.5	99.8	99.6	98.9	99.7
Mg#	0.898	0.891	0.900	0.881	0.913	0.621	0.683	0.911	0.924	0.929	0.914	0.926	0.927
Cr#						0.58	0.42	0.27	0.38	0.35	0.16	0.21	0.20
	Phlogopite				**Interstitial feldspar**				**Ti-rich oxides**		**Feldspar in spongy Cpx**		
	9501-14 av.2	9503-4 #168	9508-5 #43	9508-8 av.2	9508-1 av.2	9508-8 #3	9510-2 av.3	9510-4 #12	9508-3 Ilm.	9510-8 Arm.	9508-3 #5	9510-2 #7	9510-8 #11
SiO_2	37.22	38.12	37.73	37.92	56.73	60.10	60.96	55.51	0.09	0.17	60.84	60.25	59.96
TiO_2	2.72	4.28	7.20	4.70	0.38	0.99	0.98	0.21	56.95	72.34	0.30	0.29	1.34
Al_2O_3	17.24	16.73	16.21	16.04	25.55	24.32	24.85	26.60		2.82	23.02	24.26	25.57
Cr_2O_3	1.43	1.37	0.50	1.99	0.06	0.08	0.06	0.10	0.82	1.47	0.03	0.01	0.02
FeO	3.93	3.91	4.01	3.19	0.25	0.28	0.69	0.40	22.46	7.86	0.62	0.17	0.50
MnO	0.03	0.02	ND	0.02	0.04	0.01	0.00	0.01	0.39	0.05	0.00	0.00	0.01
MgO	20.74	20.34	19.35	20.40	0.01	0.09	0.13	0.08	16.58	13.25	0.16	0.00	0.24
CaO			0.03	0.13	7.06	0.80	1.67	8.81		0.03	0.33	4.93	0.85
Na_2O	0.69	0.70	1.03	1.12	6.58	5.24	7.12	6.22			5.45	7.69	6.72
K_2O	8.96	9.26	8.99	8.93	0.98	5.88	2.60	0.54	ND	ND	6.21	0.79	4.03
NiO	0.21	0.21	0.19	0.08	0.02		ND	ND		0.06		ND	ND
Total	93.19	94.96	95.98	94.52	97.93	97.79	99.07	98.47	98.0	98.04	96.97	98.39	99.23
Mg#	0.904	0.903	0.896	0.919					0.57	0.75			

Blank entries below detection limit. *ND* not determined. *L* large grain; *c* core; *r* rim. *Ol* olivine; *Cpx* clinopyroxene; *Spl* spinel; *Ilm* ilmenite; *Arm* armalcolite. Ol-A and Ol-B, Cpx-A and Cpx-B are individual coarse grains of Ol and Cpx or their populations with distinct compositions. 2nd, second generation grains in fine-grained aggregates inside vugs and at grain boundaries. Analyses Cpx-A and Cpx-B in sample 9510-2 are for grains labelled in Fig. 3h

peridotites (e.g. Pearson et al. 2003). A striking feature of the Al–Fe diagram (Fig. 7a) is the broad range of FeO variation (7.3–9.4%) in Tok xenoliths with a narrow range of Al_2O_3 (0.6–1.3%) and modal olivine (72–80%, not shown). Ca/Al in Tok xenoliths vary broadly as well and in many cases are much higher than in Horoman peridotites and xenoliths in kimberlites (Fig. 7b).

Mineral compositions

Table 1 of electronic supplementary material (ESM) contains EPMA data on cores of olivine, spinel and pyroxenes in all xenoliths listed in Tables 1 and 2, and four other samples. Usually, these minerals have no or only minor zoning and narrow grain-to-grain variation ranges. When pyroxene grains are zoned, their rims have higher Al and Cr than the cores; Opx rims have higher Ca while Cpx rims have lower Ca than the cores. These variations, however, are minor and only concern small mass fractions of the minerals. We believe that the average grain core analyses in Table 1 of ESM adequately characterize the main minerals of nearly all samples.

The EPMA data are compared in Figs. 9, 10, 11 and 12 with a database on over 650 spinel peridotite xenoliths and >150 abyssal peridotites (see Figs. 9, 10 for data sources). Over 100 xenoliths are from kimberlites in the Kaapvaal and Siberian cratons as well as from cratonic regions in NE China and eastern Greenland. Some 40 xenoliths are from oceanic islands. The remainder (>500) are off-craton xenoliths mainly from Siberia, Mongolia, China and North America. To identify the peridotites strongly affected by interaction with evolved melts we screened the database for samples with anomalously low Mg# in olivine ($Mg\#_{Ol}$): (a) either much lower than in fertile mantle ($Mg\#_{Ol} < 0.87$) or (b) those with low Mg# ($0.87 < Mg\#_{Ol} < 0.90$) co-existing with Cr-rich spinel ($Cr\#_{Spl} \geq 0.3$) $Cr\# = Cr/(Cr+Al)_{at}$. Because $Mg\#_{Ol}$ and $Cr\#_{Spl}$ are expected to increase sympathetically with the degree of partial melting

(Pearson et al. 2003; Walter 2003), such xenoliths were filtered out and not plotted here.

Olivine and spinel

High-precision EPMA data indicate that olivine is very homogeneous in the majority of Tok xenoliths because repeatability of individual grain analyses is close to that for the San Carlos olivine (1σ = 0.3–0.7% for Fe, 0.01–0.07% for Mg# for averages of eight points; Table 1 of ESM). Olivine is considered heterogeneous (1σ = 1–6% for Fe, 0.1–0.7% for Mg#) in 11 samples out of 32, for example FeO ranges from 9.4 to 10.3% and Mg# from 0.895 to 0.904 in olivine 9510-16. EPMA done in thin sections confirmed that olivines in those samples are zoned or have grain to grain variations (Table 3). For example, rims of coarse olivine in sample 9503-19 have lower Mg# (0.88 vs. 0.90) and NiO, and higher MnO and CaO than the cores.

The majority of Tok xenoliths (26 samples) define a tight linear correlation ($r^2 = 0.995$) between Mg#$_{Ol}$ and Mg# in whole-rocks (Mg#$_{WR}$) (Fig. 8). In the olivine-rich rocks (80% Ol), the Mg#$_{WR}$ are only slightly lower than Mg#$_{Ol}$ but the difference gradually increases to ~0.005 in the fertile lherzolites (54% Ol), consistent with modal abundances, Mg# and FeO contents of coexisting pyroxenes and spinel. Mg# of the pyroxenes are close to that in coexisting olivine or slightly higher. By contrast, spinel has much lower Mg# as well as the highest FeO among the peridotite minerals (Table 1 of ESM). As a result, spinel contribution to the Mg#$_{WR}$ usually outweighs those of the coexisting pyroxenes in spite of its low modal abundances. The difference between the Mg#$_{Ol}$ and Mg#$_{WR}$ increases from refractory to fertile Tok xenoliths (Fig. 8) in concert with spinel abundances, which rise from ~0.3% to ~2.5% (Table 1). To the best of our knowledge, these relationships between the Mg# of whole-rock mantle peridotites and their minerals have not as yet been demonstrated in detail. Six xenoliths, which plot off the trend in Fig. 8, have strongly heterogeneous olivines; half of them contain phlogopite or amphibole.

Mg#$_{Ol}$ in the majority of Tok xenoliths is positively correlated with NiO and negatively correlated with MnO; the fields of abyssal peridotites and cratonic xenoliths lie on extensions of those trends (Fig. 9). The contents of MnO and NiO in olivine from refractory

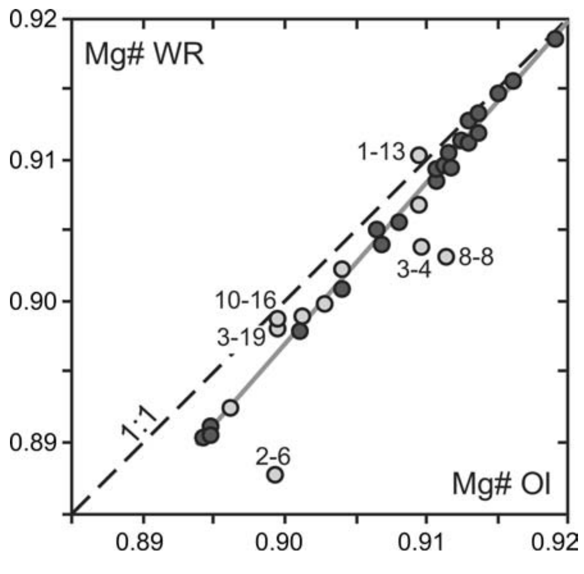

Fig. 8 Mg# Mg/(Mg + Fe)$_{at}$ in olivine versus whole-rock (WR) Mg#. The majority of the xenoliths define a very tight linear correlation (*thick grey line*; $r^2 = 0.995$) demonstrating excellent quality of the WR and EPMA data. Six labelled samples with heterogeneous olivine (see Fig. 7 and text) plot off the trend mainly because the grains analysed are not representative of the total olivine populations

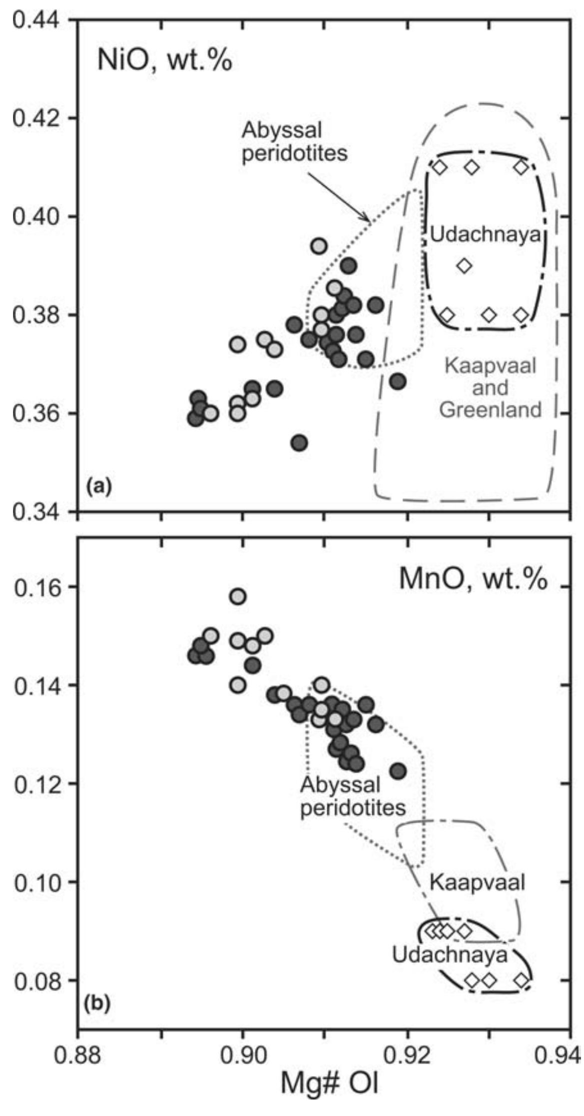

Fig. 9 Plots of Mg#$_{Ol}$ vs. NiO (**a**) and MnO (**b**) in olivine. Also shown are fields for abyssal peridotites (Hellebrand et al. 2001) and spinel peridotites from Udachnaya (Boyd et al. 1997), the Kaapvaal craton (Boyd et al. 1999; Smith 2000) and East Greenland (Bernstein et al. 1998)

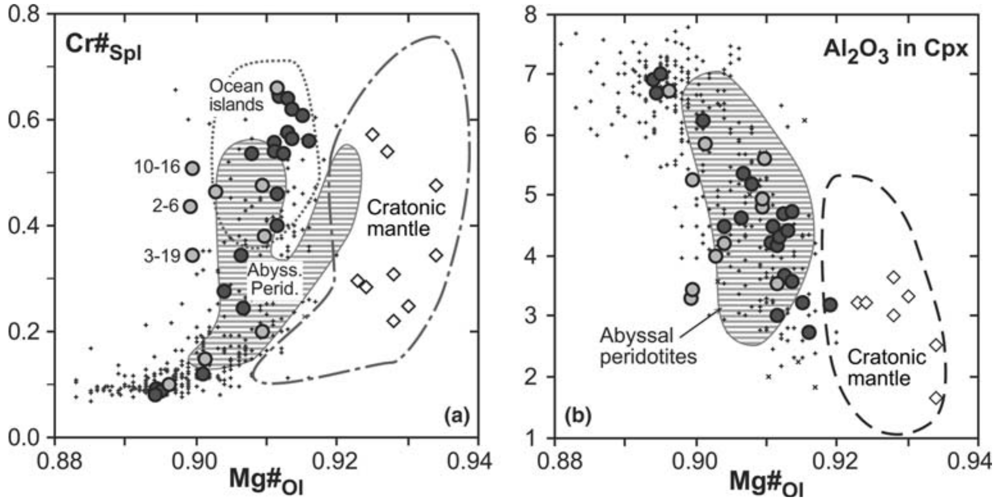

Fig. 10 Plots of $Mg\#_{Ol}$ vs. $Cr\#_{Spl}$ $Cr/(Cr+Al)_{at}$ (**a**) and Al_2O_3 (wt.%) in Cpx (**b**) in mantle spinel peridotites. Symbols are same as in Fig. 7. Data sources in addition to those in Figs. 4, 5, 6, 7, 8, 9 are: cratons, Zheng et al. (2001); continental off-craton areas, Ionov et al. (1992a, 1995a, 1995b), Smith (2000), Zhang et al. (2000), and Xu et al. (2003); ocean islands, Hauri and Hart (1994), Grégoire et al. (2000), and Neumann et al. (2002); abyssal peridotites, Johnson et al. (1990), Dick and Natland (1996), Niida (1997), and Ross and Elthon (1997)

Tok xenoliths overlap the field of abyssal peridotites. The Tok olivines typically have lower NiO and higher MnO than those in the Kaapvaal and Udachnaya peridotites. The xenolith literature data show a broad scatter on Mg#–Ni–Mn plots mainly due to the insufficient accuracy of routine EPMA.

$Cr\#_{Spl}$ ranges from 0.08 in fertile Tok xenoliths to 0.65 in highly refractory rocks and is positively correlated with $Mg\#_{Ol}$ (Fig. 10a), consistent with partial melting relationships in residual peridotites (Hellebrand et al. 2001; Pearson et al. 2003; Smith 2000). The majority of the Tok xenoliths plot in the middle of the off-craton peridotite field in Fig. 10a and have lower $Mg\#_{Ol}$ than the xenoliths from Udachnaya and the Kaapvaal craton at similar $Cr\#_{Spl}$. The literature data show a fairly broad range of $Mg\#_{Ol}$ at similar $Cr\#_{Spl}$ in the off-craton peridotites, e.g. from 0.905 to 0.925 at $Cr\#_{Spl} \geq 0.3$ (Fig. 10a). To some extent, the Mg# scatter can be attributed to the insufficient accuracy of routine EPMA data in combination with a narrow Mg# variation range (0.89–0.92). On the other hand, the Mg# variations may result from differences in the depth of partial melting (Walter 2003; Herzberg 2004) as well as metasomatic Fe-enrichment (as for several Tok xenoliths with heterogeneous olivine, Fig. 10a). Overall, $Cr\#_{Spl}$ may be a more robust index of melt extraction rates in mantle peridotites than $Mg\#_{Ol}$ (Hellebrand et al. 2001).

Clinopyroxene

Cpx in the Tok xenoliths has the same range of Al_2O_3 as abyssal peridotites but much higher Na_2O (Figs. 10b, 11a, 12). Exceptionally high Na_2O contents (2.2–3.1%) are typical for the Cpx from refractory ($Cr\#_{Spl} > 0.25$) Tok xenoliths and are consistent with high whole-rock Na_2O (Fig. 6c). The common Na-rich Cpx is a remarkable feature of the Tok peridotites, which can only be matched by some kimberlite-hosted xenolith suites (Bizzarro and Stevenson 2003). Very high Na_2O (2–4%) were occasionally reported for Cpx in other peridotites, e.g. those with glass pockets (Ionov et al. 1994), but such rocks are rare in most other xenolith suites.

Nearly all Na-rich Tok Cpx have high Cr_2O_3 (2–3.5%) and can be distinguished on the Cr–Na diagram from Cpx in most other peridotites in our database (Fig. 12). By contrast to Na and Cr, the contents of TiO_2 in Cpx from refractory Tok xenoliths are moderate ($\leq 0.25\%$) and hence closer to those for other mantle peridotites (Fig. 11b). A Na–Ti plot outlines a particular field of Na-rich, Ti-poor Cpx, which are rare in other peridotite suites (Fig. 12a).

Accessory and second-generation minerals

Fine-grained, second-generation olivine, Cpx and spinel in the Tok xenoliths (e.g. Fig. 3g–h) have distinctive compositions. Second-generation olivine typically has higher Mg# and CaO and lower NiO than primary olivine, including rocks with zoned olivine (Table 3). Second-generation spinel usually has higher FeO and TiO_2 than primary spinel and a broad range of Cr#. Second-generation Cpx typically has lower Na_2O and higher TiO_2 than primary Cpx and significant Al_2O_3 and Cr_2O_3 grain-to-grain variations. Spongy Cpx is particularly low in Na and Al (Table 3).

Phlogopite has a broad range of TiO_2 and typically low totals, which indicate the presence of volatile components (OH^-, O^{2-}, F, Cl) (Ionov et al. 1997). Feldspar, both interstitial and that replacing (together with second-generation Ol, Cpx and Spl) phlogopite and amphibole is alkali-rich regardless of its textural position, with 5–8% Na_2O and 0.5–7% K_2O (Table 3). The CaO contents range broadly (0–9%) but usually are low. Importantly, no Ca-rich plagioclase has been found. Feldspar analyses usually yield high TiO_2 and FeO, which in some cases may be related to micro-inclusions of (Fe,Ti)-rich oxides. Ilmenite, armalcolite and rutile have been identified among the small number of oxide

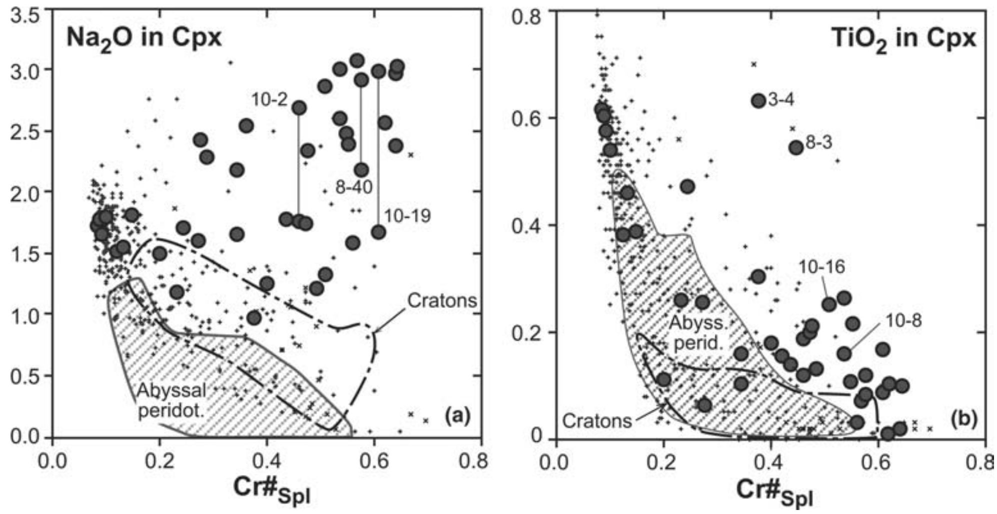

Fig. 11 Plots of Cr#$_{Spl}$ vs. Na_2O (**a**) and TiO_2 (**b**) in Cpx (wt.%) from mantle spinel peridotites. Data sources are same as in Fig. 10. Two populations of coarse Cpx are plotted for Tok xenoliths 9508-40, 9510-2 and 9510-19; each pair of points is connected with *thin grey lines* in (**a**). High Na_2O and low to moderate TiO_2 contents are common in Tok Cpx

grains analysed in this study. Overall, the mineral associations and compositions of the feldspar–Ti-oxide assemblage do not appear to be different from those in other mantle xenolith suites in southern Siberia, in which this type of mantle metasomatism is widespread (Ionov et al. 1995b, 1999; Kalfoun et al. 2002).

Temperature (*T*) and pressure (*P*) estimates

Equilibration temperatures estimated from the EPMA using the Ca-in-opx method of Brey and Köhler (1990) range from 870°C to 1,020°C (Table 1). Fertile xenoliths (Cr#$_{Spl}$ < 0.2) yield highest *T* estimates (964–1,010°C). *T* values are negatively correlated with Cr#$_{Spl}$ (Fig. 13) indicating that refractory peridotites tend to be 'colder'. Assuming that temperature regularly increases with depth, the proportion of refractory rocks must be higher in the shallow CLM. The fertile peridotites may be absent from the depth range corresponding to *T*-range 870–950°C.

The depth of origin for the xenoliths cannot be estimated directly because of the lack of reliable barometers for spinel peridotites. The absence of garnet in fertile Tok lherzolites at ~1,000°C indicates that equilibration pressures for those rocks do not exceed 18 kbar (Brey and Köhler 1990; Ionov et al. 2005 and references therein) and hence their depth of origin is ≤ 60 km. Because the fertile rocks appear to be the deepest among the Tok xenoliths, all of them may have been brought up from depths ≤ 60 km. The presence of metasomatic feldspar in some Tok xenoliths does not mean that those rocks are shallow plagioclase facies peridotites because the feldspar is alkali-rich (Table 3) and hence distinct from the Ca-rich plagioclase in peridotite massifs, as discussed earlier by Ionov et al. (1995b) for xenoliths from southern Baikal region. Moreover, the feldspar usually occurs locally in small interstitial aggregates and breakdown products of amphibole and phlogopite but does not replace primary spinel (Fig. 3a, b, d, e).

The lowest *T* estimates for the Tok xenoliths (~880°C) are identical to those obtained using the same

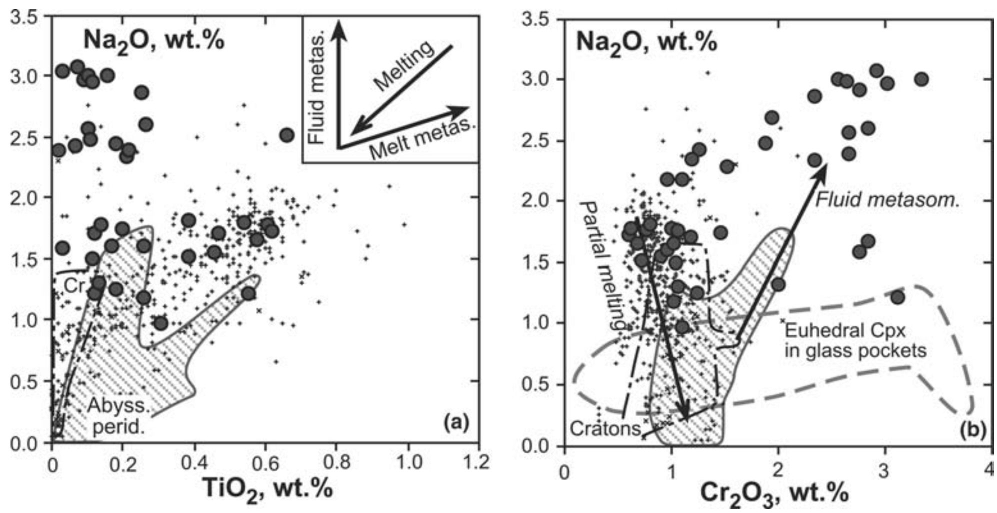

Fig. 12 Plots of Na_2O vs. TiO_2 (**a**) and Cr_2O_3 (**b**) in Cpx (**b**) from mantle spinel peridotites. Symbols and data sources are same as in Fig. 10. Also shown in (**b**) is a field for Cpx microphenocrysts in silicate glass pockets in mantle xenoliths (Ionov et al. 1994; Chazot et al. 1996; Neumann and Wulff-Pedersen 1997; Vannucci et al. 1998; Laurora et al. 2001; Bali et al. 2002). *Arrows* show melting trends for abyssal peridotites (Hellebrand et al. 2001) and those inferred for 'fluid' (high Na, low Ti) and 'melt' (Ti-rich, low to moderate Na) metasomatism

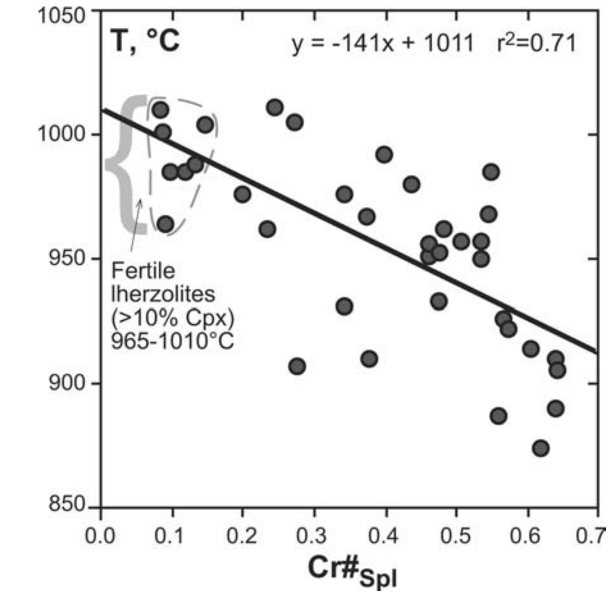

Fig. 13 Equilibration temperatures (T) after Brey and Köhler (1990) plotted versus Cr#$_{Spl}$. The refractory peridotites tend to have lower equilibration T's and hence may be more common at lower depths than the fertile peridotites

method for spinel peridotite xenoliths in late Cenozoic volcanic rocks south of the Siberian craton: Vitim (Fig. 1a) and Tariat in central Mongolia (Ionov et al. 1998, 2005). Geothermal gradients and lithospheric sections for these two sites are well established from P–T data on garnet-bearing xenoliths. If the geothermal gradient in the uppermost Tok CLM is similar, the Tok xenoliths may come from the depth range 40–60 km. One should keep in mind however that magmatic underplating in the Tok CLM, which produced cumulate and composite xenoliths, may have perturbed the geothermal gradients.

Trace element compositions of whole-rock peridotites

The whole-rock solution ICPMS analyses for ten xenoliths are given in Table 2 of ESM. Fertile lherzolites have nearly flat REE patterns (normalized to primitive mantle, PM), with heavy to medium REE abundances close to PM values (Fig. 14a). Refractory Tok peridotites have much lower HREE (0.1–0.4 times PM) indicating higher rates of melt extraction and show a gradual increase in less compatible REE. The shapes of their REE patterns differ significantly, with La/Yb$_{PM}$ ranging from 2 to 40 (Fig. 14a). Five out of seven LREE-enriched xenoliths have strong negative anomalies of high field strength elements (HFSE: Ti, Zr, Hf, Nb) (Fig. 14b) and contain >0.1% of modal phosphates. Such features are usually attributed to "carbonatite-type" metasomatism (see Ionov et al. (2002) for references and discussion).

The host lava has no negative HFSE anomalies but shows a Nb spike (Fig. 14a). The low HFSE in many xenoliths and big differences in trace element ratios (as well as K/Na and K/P from XRF data) with the host basalt rule out significant entrapment of host magma before or during the eruption. Hence, the fine-grained interstitial materials (including feldspar, Ti-rich oxides, phosphates) were formed by metasomatism of the peridotites before they were captured by the magma. The variety of trace element patterns in the peridotites indicates that the rocks experienced different degrees of enrichment by a range of metasomatic media.

Fig. 14 **a, b** Primitive mantle-normalized (Hofmann 1988) REE (**a**) and multi-element (**b**) abundance patterns of six representative LH series xenoliths and host basalt. The refractory xenoliths are enriched in LREE but have different patterns indicating different styles and degrees of metasomatism. Distinct element patterns and ratios in the xenoliths and the host basalt rule out significant contamination of the xenoliths with the host magma

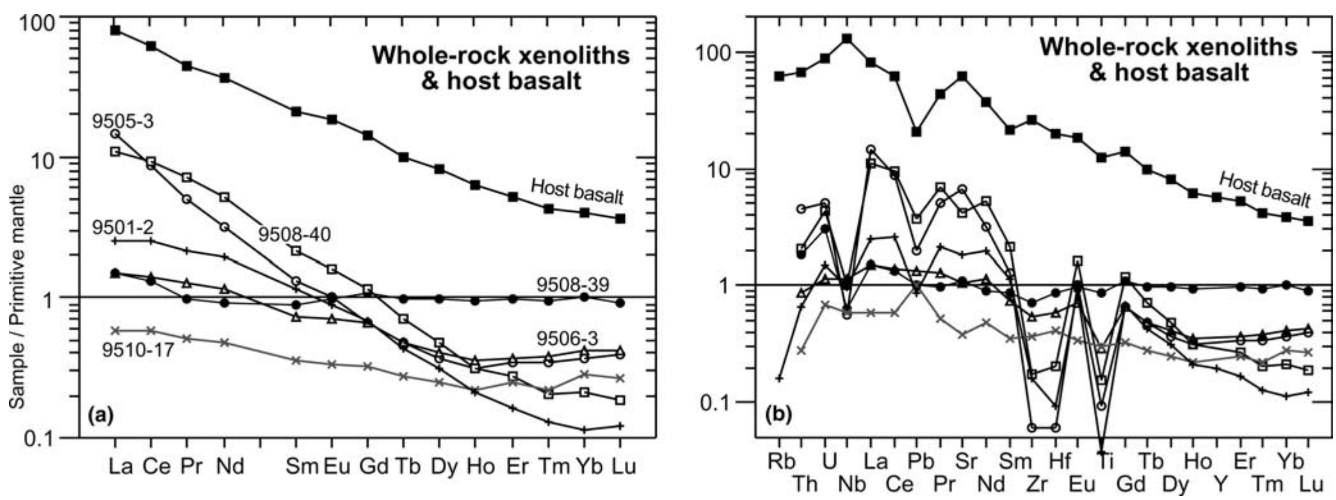

Discussion

We focus on the following topics: (1) the creation of a protolith for the Tok CLM by melt extraction from fertile mantle, (2) the role of partial melting and later

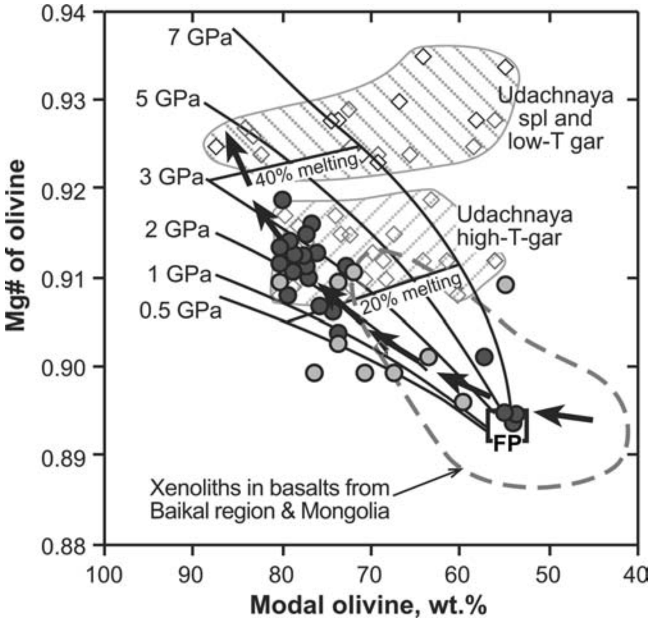

Fig. 15 A plot of $Mg\#_{Ol}$ versus modal olivine ("Boyd diagram") for Tok LH series xenoliths. Also shown are peridotites from Udachnaya in central Siberian craton (Boyd et al. 1997) and xenoliths in basalts from central Asia (see Fig. 10 for data sources). *Solid black lines* are batch partial melt extraction residues from fertile peridotite (FP) at 0.5–7 GPa (Walter 1999, 2003)

events in the origin of Tok peridotites, and (3) heterogeneity of the CLM beneath the Siberian craton.

Effects of metasomatism on modal and chemical compositions

We first seek to identify Tok xenoliths affected by metasomatism and constrain modal and chemical compositions of the initial melting residues. As noted above, Al_2O_3 may be the least affected among the major oxides by post-melting events, like precipitation of late-stage Cpx and phosphates. Nearly all Tok xenoliths plot close to experimental melt extraction trends and the Horoman field on the Mg-Al plot (Fig. 5a). By contrast, some refractory Tok xenoliths have higher Cpx at similar modal olivine (Fig. 4a) and higher Ca/Al at similar Al_2O_3 (Fig. 7b) than Horoman and cratonic peridotites apparently due to the significant late-stage Cpx. Furthermore, several Tok xenoliths have Fe-enrichments in olivine (Fig. 10a) and bulk rocks (Figs. 5b, 7a) relative to melting residues and the Horoman peridotites. Importantly, the enrichments in Fe (and Mn) do not always match those in modal Cpx and high Ca/Al and hence may result from different metasomatic events (cf. Fig. 7a, b). Sample 9510-16 is enriched both in Cpx and FeO but xenoliths 9505-3 and 9501-13 with relatively high modal Cpx (Fig. 4a) and Ca/Al (Fig. 7b) do not show significant enrichments in iron (Figs. 5b, 7a). By contrast, samples 9508-3 (Fig. 3c) and 9502-6 are enriched in iron but have moderate Cpx and Ca/Al.

Some other petrographic and chemical data confirm that the metasomatism was a complex, multi-stage process with a range of melt/fluid compositions. Cpx in many refractory Tok samples has a slightly to moderately high Ti relative to melting trends (Hellebrand et al. 2001), abyssal peridotites and many cratonic peridotites (Fig. 11b). Highest TiO_2 are in Cpx from phlogopite-bearing xenoliths and those enriched in iron. The commonly high Na_2O in Tok Cpx (well above those for abyssal peridotites at similar Cr_{Spl}, Fig. 11a) was certainly produced by metasomatism, but the enrichments in Na do not correlate with those in Fe and Ti (Fig. 12a). Several xenoliths contain Cpx populations with different Na_2O (Figs. 3h, 11a). Moreover, a combination of high Na and Cr contents, typical of Tok Cpx (Fig. 12b), is not likely to be a result of equilibration with any known type of mantle-derived magmatic liquid. For example, Cpx micro-phenocrysts in pockets of Na-rich glass in many mantle xenolith suites have low to moderate Na_2O ($<1.2\%$, Fig. 12b), consistent with low Cpx/melt partition coefficients for Na at low pressures (Blundy et al. 1995; Hellebrand and Snow 2003; Takazawa et al. 2000; Walter 2003). Hence, the high Na_2O in Tok Cpx appear to be related to metasomatism by Na-rich fluids rather than melts. We conclude that some residual Tok peridotites first experienced percolation of various evolved liquids, which caused precipitation of Cpx, hydrous minerals and enrichments in Fe, Mn and Ti. Those events were followed by alkali-rich fluid metasomatism, which affected Cpx and produced feldspar- and phosphate-bearing interstitial materials and strong LREE enrichments.

Partial melting in the Tok CLM

Modal and chemical data on residual peridotites shed light on partial melting events that depleted the 'fusible' components in the primordial mantle. The degree and the character of the depletion are mainly controlled by melting conditions, which in turn are related to the lithospheric ages and tectonic settings (Pearson et al. 2003; Walter 2003). A characteristic feature of the ancient cratonic mantle worldwide is that it is strongly depleted in 'basaltic' components.

Apart from metasomatic effects constrained in the previous section, the abundances of Cpx, major oxides and the compatible to moderately incompatible elements in the majority of Tok xenoliths, as well as olivine compositions, vary systematically with variations in modal olivine, MgO and Mg# (Figs. 4, 5, 6, 7, 8, 9, 14a). Such relationships are commonly seen as evidence that the peridotites formed as residues after variable degrees of partial melting and melt extraction from fertile lherzolite sources. The Tok xenoliths usually plot on major oxide plots (Figs. 5, 6, 7) close to evolution lines for residues of polybaric fractional melting at low to moderate pressures (≤ 3 GPa) (Niu 1997; Walter 2003; Herzberg 2004) and fall within the compositional field of the Horoman peridotites inferred to have been derived by polybaric melting at 2.5–0.4 GPa (Takazawa et al. 2000). The Tok xenoliths also fit model residues of batch melting at 1–3 GPa (Walter 1999, 2003) on plots of MgO versus FeO (Fig. 5b) and of modal olivine vs. $Mg\#_{Ol}$ (Fig. 15).

Further constraining the melting conditions of the Tok peridotites may be difficult due to the variable Fe-enrichments and because the melting may have taken place at a range of depths. It is essential, however, that the experimental data clearly indicate relatively low melting pressures (1–3 GPa), which contrast sharply with much higher values (> 3 GPa) inferred for kimberlite-hosted peridotites from central Siberian craton (Fig. 15) and South Africa (Walter 2003; Herzberg 2004). Differences with other cratonic sites and similarities with off-craton mantle are also evident from major element compositions of minerals, e.g. on plots of $Mg\#_{Ol}$ versus $Cr\#_{Spl}$ or Al_2O_3 in Cpx (Fig. 10). Thus, the melting conditions for the Tok suite may have been similar to those for peridotite massifs and xenoliths from continental off-craton regions and oceanic islands. Higher proportion of refractory peridotites in the Tok LH series than in most off-craton suites implies higher melt extraction rates (up to 25–40%; Herzberg 2004). Collectively, the petrographic, modal and chemical data on Tok xenoliths, together with experimental results, indicate that their protoliths were produced by melt extraction at low ($\leq$ 3 GPa) pressures.

Compositional variations in the lithospheric mantle in central and northern Asia

Early Russian data on peridotite xenoliths from the Anabar block (Sobolev 1977; Spetsius and Serenko 1990; Ukhanov et al. 1988) indicated broad similarities between the CLM in the Siberian and Kaapvaal cratons, like a combination of high Mg# and low Mg/Si. These similarities were further demonstrated using geochemical data on peridotite xenoliths from Udachnaya (Boyd et al. 1997; Pearson et al. 1995). By contrast, many recent xenolith studies worldwide documented significant chemical and modal differences between peridotite suites from different cratons as well as within individual cratons (e.g. Bernstein et al. 1998; Kelemen et al. 1998; Kopylova and Russell 2000; Pearson et al. 2003; Schmidberger and Francis 1999). Studies of mineral concentrates from several Yakutian kimberlite fields have outlined compositional variations also within the CLM in the Anabar block (Griffin et al. 1999).

Because refractory peridotites are dominant among the Tok xenoliths, they are similar in this regard to cratonic xenoliths from central Siberia and elsewhere (Boyd et al. 1997; Pearson et al. 2003). On the other hand, the Tok LH series rocks have lower Mg# and less variable (but typically lower) modal Opx than coarse peridotites from Udachnaya and other kimberlites in central Siberia and plot close to the 'oceanic' melting trend on the "Boyd diagram" (Fig. 15). The refractory Tok peridotites also have higher MnO in olivine and usually higher modal Cpx than the Udachnaya xenoliths. Even though some of the latter contain late-stage interstitial Cpx (Boyd et al. 1997), its abundances are normally lower than in the Tok xenoliths (Fig. 4a). Overall, the data on the Tok xenoliths indicate significant differences in modal and chemical composition between the CLM in central and south-eastern parts of the Siberian craton. On the other hand, the Tok peridotites are generally more refractory (and have higher Na in Cpx) than off-craton xenolith suites from nearby southern Siberia and Mongolia (Figs. 4, 5, 6, 7, 10, 11, 12).

The protolith for the Tok xenoliths may have formed in the late Archean-Paleoproterozoic if the CLM beneath Tok has been coupled with the overlying crust since its origin. Compared to xenoliths from the older (Paleozoic–Mesozoic) kimberlites in the central Siberian craton, the xenoliths from Tok (hosted by late Cenozoic basalts) may bear evidence of Mesozoic–Cenozoic events in the CLM, e.g. those related to subduction in the Pacific oceanic basin in the east. The apparent lack of the cratonic keel and the widespread petrographic and chemical signatures of metasomatism in the Tok CLM may be related to those recent events.

The Siberian craton is commonly considered as a single unit, and tectonic reconstructions usually assume that the Aldan shield has been part of the craton at least since 2 Ga (Condie and Rosen 1994). However, some new paleomagnetic data as well as a re-assessment of earlier work (Kravchinsky et al. 2001; Smethurst et al. 1998) indicate that SE Siberia was rotated ~20° relative to central Siberia along the Vilyui basin (Fig. 1a) in mid-Paleozoic, and that there's not enough reliable data to establish exactly pre-Devonian path of the Anabar block. Given the uncertain tectonic contiguity of the craton, as well as differences in the Precambrian and Phanerozoic geologic history (Rosen et al. 1994), there is no reason why the composition of the CLM in the SE and northern parts of the Siberian craton should be identical. Furthermore, the CLM within the Aldan-Stanovoy and Angara blocks (Fig. 1a) may be heterogeneous as well because they formed by amalgamation of smaller terranes (e.g., Pisarevsky and Natapov 2003).

Summary of conclusions

1. Peridotite xenoliths in Cenozoic basalts from Tok are the only known suite of basalt-borne mantle samples from the Siberian craton. The extensive and detailed petrographic, modal and chemical results on those xenoliths produced in this study provides the first comprehensive dataset on the CLM in the Aldan–Stanovoy block of the craton and shows significant differences with the CLM beneath the central and northern parts of the craton (Anabar block).

2. The absence of garnet and plagioclase facies peridotites among the Tok xenoliths as well as comparisons with well-established *P–T* gradients for nearby off-craton sites, indicates the provenance from a depth range 40–60 km, i.e. within the shallow, uppermost CLM. Equilibration temperatures of the Tok peridotites (870–1,020°C) are much higher than at similar depths in the central Siberian craton indicating either a much thinner lithosphere or massive recent underplating of basaltic melts in the shallow mantle, which perturbed the local geotherm. The CLM in the Tok area almost certainly has no cratonic keel, which either never existed or has been delaminated. The CLM beneath Tok may be chemically stratified because fertile peridotites appear to occur only in the deeper part of the lithospheric section.
3. The lherzolite–harzburgite series rocks are most common among the Tok xenoliths and appear to represent mantle wall-rock peridotites initially produced by partial melting. The LH series is dominated by olivine-rich, refractory peridotites indicating that the protolith for the uppermost CLM beneath the SE margin of the Siberian craton was created by high degrees of melt extraction (up to 25–40%) from a fertile source. In that regard, the Tok xenolith suite is typical of the CLM beneath cratons and distinct from adjacent off-craton mantle domains.
4. Modal and major oxide compositions of the Tok peridotites are consistent with an origin by partial melting at generally lower pressures (≤ 3 GPa) than those inferred for kimberlite-hosted xenoliths from the central Siberian craton. Furthermore, the Tok xenoliths do not have high modal orthopyroxene and low Mg/Si values common for peridotites from central Siberian craton. Altogether, our data indicate large-scale modal and chemical heterogeneities of the CLM beneath the Siberian craton, possibly related to differences in formation conditions, geologic history and tectonic settings.
5. The initial melting residues in the Tok CLM were extensively metasomatized by different media. Evolved silicate melts produced enrichments in Fe and replacement of orthopyroxene by clinopyroxene while fluid-related metasomatism is indicated by strong enrichments in Na. The metasomatism may be related to the position near the margin of the craton affected by large-scale tectono-magmatic events in the Mesozoic and Cenozoic.

Acknowledgements A. Kokovkin, M. Vikhtenko and M. Goroshko took part in the fieldwork. DAI thanks T. Bradley, G. Chazot, K. Furuta, N. Groschopf, D. Kuzmin, C. Merlet, E. Takazawa and M. Veschambre for assistance with sample preparation and analytical work. The fieldwork was organized by ITIG, Far Eastern Branch of the Russian Academy of Sciences. DAI's trip to Siberia was funded by the Australian Research Council. The study was supported by funding from Fond Nationale de la Recherche Scientifique (FNRS – grant# FRFC: 2.4607.01 F) and Université Libre de Bruxelles (Belgium), Université de Montpellier II and Université Blaise Pascal (France), MPI-Chemie in Mainz as well as a W.Paul Award of the A.von Humboldt Foundation (Germany) to AVS. Some ICPMS analyses were done using the funding and facilities of the European Geochemical Facility at Bristol in 2002.

References

Bali E, Szabo C, Vaselli O, Torok K (2002) Significance of silicate melt pockets in upper mantle xenoliths from the Bakony-Balaton Highland Volcanic Field, Western Hungary. Lithos 61:79–102

Bernstein S, Kelemen PB, Brooks CK (1998) Depleted spinel harzburgite xenoliths in Tertiary dykes from East Greenland: restites from high degree melting. Earth Planet Sci Lett 154:219–233

Bizzarro M, Stevenson RK (2003) Major element composition of the lithospheric mantle under the North Atlantic craton: evidence from peridotite xenoliths of the Sarfartoq area, southwestern Greenland. Contrib Mineral Petrol 146:223–240

Blundy JD, Falloon TJ, Wood BJ, Dalton JA (1995) Sodium partitioning between clinopyroxene and silicate melts. J Geophys Res 100:15501–15515

Boyd FR, Pokhilenko NP, Pearson DG, Mertzman SA, Sobolev NV, Finger LW (1997) Composition of the Siberian cratonic mantle: evidence from Udachnaya peridotite xenoliths. Contrib Mineral Petrol 128:228–246

Boyd FR, Pearson DG, Mertzman SA (1999) Spinel-facies peridotites from the Kaapvaal root. In: Gurney JJ, Gurney JL, Pascoe MD, Richardson SH (eds) Proceedings of the 7th international kimberlite conference, vol 1. RedRoof Design, Cape Town, pp 40–48

Brey GP, Köhler T (1990) Geothermobarometry in four-phase lherzolites. II. New thermobarometers, and practical assessment of existing thermobarometers. J Petrol 31:1353–1378

Chazot G, Menzies M, Harte B (1996) Silicate glasses in spinel lherzolites from Yemen: origin and composition. Chem Geol 134:159–179

Condie KC, Rosen OM (1994) Laurentia–Siberia connection revisited. Geology 22:168–170

Dick HJB, Natland JH (1996) Late-stage melt evolution and transport in the shallow mantle beneath the East Pacific Rise. Proc ODP Sci Res 147:103–134

Francis D (1987) Mantle-melt interaction recorded in spinel lherzolite xenoliths from the Alligator Lake volcanic complex, Yukon, Canada. J Petrol 28:569–597

Frey FA, Green DH (1974) The mineralogy, geochemistry and origin of lherzolite inclusions in Victorian basanites. Geochim Cosmochim Acta 38:1023–1059

Frost BR, Avchenko OV, Chamberlain KR, Frost CD (1998) Evidence for extensive Proterozoic remobilisation of the Aldan shield and implications for Proterozoic plate tectonic reconstructions of Siberia and Laurentia. Precambrian Res 89:1–23

Grégoire M, Moine BN, O'Reilly SY, Cottin JY, Giret A (2000) Trace element residence and partitioning in mantle xenoliths metasomatised by highly alkaline, silicate- and carbonate-rich melts (Kerguelen Islands, Indian Ocean). J Petrol 41:477–509

Griffin WL, Ryan CG, Kaminsky FV, O'Reilly SY, Natapov LM, Win TT, Kinny PD, Ilupin IP (1999) The Siberian lithosphere traverse: mantle terranes and the assembly of the Siberian craton. Tectonophysics 310:1–35

Gusev GS, Khain VE (1995) Relationships between Baikalo-Vitim, Aldan-Stanovoy and Mongol-Okhotsk terrains (South Siberia) (in Russian). Geotectonics Sept/Oct:68–82

Harte B (1977) Rock nomenclature with particular relation to deformation and recrystallisation textures in olivine-bearing xenoliths. J Geol 85:279–288

Hauri EH, Hart SR (1994) Constraints on melt migration from mantle plumes: a trace element study of peridotite xenoliths from Savai'i, Western Samoa. J Geophys Res 99:24301–24321

Hellebrand E, Snow JE (2003) Deep melting and sodic metasomatism underneath the highly oblique-spreading Lena Trough (Arctic Ocean). Earth Planet Sci Lett 216:283–299

Hellebrand E, Snow JE, Dick HJB, Hofmann AW (2001) Coupled major and trace elements as indicators of the extent of melting in mid-ocean-ridge peridotites. Nature 410:677–681

Herzberg C (2004) Geodynamic information in peridotite petrology. J Petrol 45:2507–2530

Hofmann AW (1988) Chemical differentiation of the Earth: the relationship between mantle, continental crust and oceanic crust. Earth Planet Sci Lett 90:297–314

Ionov D (2002) Mantle structure and rifting processes in the Baikal-Mongolia region: geophysical data and evidence from xenoliths in volcanic rocks. Tectonophysics 351:41–60

Ionov DA, Kramm U, Stosch H-G (1992a) Evolution of the upper mantle beneath the southern Baikal rift zone: a Sr–Nd isotope study of xenoliths from the Bartoy volcanoes. Contrib Mineral Petrol 111:235–247

Ionov DA, Savoyant L, Dupuy C (1992b) Application of the ICP-MS technique to trace element analysis of peridotites and their minerals. Geostandard Newslett 16:311–315

Ionov DA, Hofmann AW, Shimizu N (1994) Metasomatism-induced melting in mantle xenoliths from Mongolia. J Petrol 35:753–785

Ionov DA, Prikhod'ko VS, O'Reilly SY (1995a) Peridotite xenoliths from the Sikhote-Alin, south-eastern Siberia, Russia: trace element signatures of mantle beneath a convergent continental margin. Chem Geol 120:275–294

Ionov DA, O'Reilly SY, Ashchepkov IV (1995b) Feldspar-bearing lherzolite xenoliths in alkali basalts from Hamar-Daban, southern Baikal region, Russia. Contrib Mineral Petrol 122:174–190

Ionov DA, O'Reilly SY, Griffin WL (1997) Volatile-bearing minerals and lithophile trace elements in the upper mantle. Chem Geol 141:153–184

Ionov DA, O'Reilly SY, Griffin WL (1998) A geotherm and lithospheric cross-section for central Mongolia. In: Flower MJF, Chung S-L, Lo C-H, Lee TY (eds) Mantle dynamics and plate interactions in East Asia. Amer Geophys Union, Geodynamics Series 27, Washington DC, pp 127–153

Ionov DA, Grégoire M, Prikhod'ko VS (1999) Feldspar–Ti-oxide metasomatism in off-cratonic continental and oceanic upper mantle. Earth Planet Sci Lett 165:37–44

Ionov DA, Bodinier J-L, Mukasa SB, Zanetti A (2002) Mechanisms and sources of mantle metasomatism: major and trace element compositions of peridotite xenoliths from Spitsbergen in the context of numerical modeling. J Petrol 43:2219–2259

Ionov DA, Ashchepkov I, Jagoutz E (2005) The provenance of fertile off-craton lithospheric mantle: Sr–Nd isotope and chemical composition of garnet and spinel peridotite xenoliths from Vitim, Siberia. Chem Geol 217:41–75

Jahn B-M, Gruau G, Capdevila R, Cornichet J, Nemchin A, Pidgeon R, Rudnik VA (1998) Archean crustal evolution of the Aldan shield, Siberia: geochemical and isotopic constraints. Precambrian Res 91:333–363

Jarosewich E, Nelen JA, Norberg J (1980) Reference samples for electron microprobe analysis. Geostandard Newslett 4:43–47

Johnson KTM, Dick HJB, Shimizu N (1990) Melting in the oceanic upper mantle: an ion probe study of diopsides in abyssal peridotites. J Geophys Res 95:2661–2678

Kalfoun F, Ionov D, Merlet C (2002) HFSE residence and Nb–Ta ratios in metasomatised, rutile-bearing mantle peridotites. Earth Planet Sci Lett 199:49–65

Kelemen PB, Hart SR, Bernstein S (1998) Silica enrichment in the continental upper mantle via melt/rock reaction. Earth Planet Sci Lett 164:387–406

Kiselev AI, Medvedev ME, Golovko GA (1979) Volcanism of the Baikal rift zone and problems of deep magma generation (in Russian). Nauka, Novosibirsk, 197 p

Kogarko LN, Semenova VG, Solov'yeva LV, Kolesov GM, Shubina NA, Korovkina NA (1990) Geochemistry of the upper mantle under the south rim of the Aldan shield. Trans (Doklady) Acad Sci USSR, Earth Sci Sect 303:206–209

Kopylova MG, Russell JK (2000) Chemical stratification of cratonic lithosphere: constraints from the Northern Slave craton, Canada. Earth Planet Sci Lett 181:71–87

Kravchinsky VA, Konstantinov KM, Cogne J-P (2001) Palaeomagnetic study of Vendian and Early Cambrian rocks of South Siberia and Central Mongolia: was the Siberian platform assembled at this time? Precambrian Res 110:61–92

Laurora A, Mazzucchelli M, Rivalenti G, Vannucci R, Zanetti A, Barbieri MA, Cingolani CA (2001) Metasomatism and melting in carbonated peridotite xenoliths from the mantle wedge: the Gobernador Gregores case (southern Patagonia). J Petrol 42:69–87

Lee C-T, Rudnick RL (1999) Compositionally stratified cratonic lithosphere: petrology and geochemistry of peridotite xenoliths the Labait volcano, Tanzania. In: Gurney JJ, Gurney JL, Pascoe MD, Richardson SH (eds) Proceedings of the 7th international kimberlite conference, vol 1. RedRoof Design, Cape Town, pp 503–521

Merlet C (1994) An accurate computer correction program for quantitative electron probe microanalysis. Mikrochim Acta 114(115):363–376

Neumann E-R, Wulff-Pedersen E (1997) The origin of highly silicic glass in mantle xenoliths from the Canary Islands. J Petrol 38:1513–1539

Neumann E-R, Wulff-Pedersen E, Pearson NJ, Spenser EA (2002) Mantle xenoliths from Tenerife (Canary Islands): evidence for reactions between mantle peridotites and silicic carbonatite melts inducing Ca metasomatism. J Petrol 43:825–857

Niida K (1997) Mineralogy of MARK peridotites: replacement through magma channeling examined from Hole 920D, MARK area. Proc ODP Sci Res 153:265–275

Niu Y (1997) Mantle melting and melt extraction processes beneath ocean ridges: evidence from abyssal peridotites. J Petrol 38:1047–1074

Nutman AP, Chernyshev IV, Baadsgaard H, Smelov AP (1992) The Aldan shield of Siberia, USSR: the age of its Archean components and evidence for widespread reworking in the mid-Proterozoic. Precambrian Res 54:195–210

Palme H, O'Neill HSC (2003) Cosmochemical estimates of mantle composition. In: Carlson RW (ed) Treatise on geochemistry, vol 2. The mantle and core. Elsevier, Amsterdam, pp 1–38

Parfenov LM, Kosmin BM, Imaev VS, Savostin LA (1987) The tectonic character of the Olekma–Stanovoy seismic zone. Geotectonics 21:560–572

Pearson DG, Shirey SB, Carlson RW, Boyd FR, Pokhilenko NP, Shimizu N (1995) Re–Os, Sm–Nd, and Rb–Sr isotope evidence for thick Archaean lithospheric mantle beneath the Siberian craton modified by multistage metasomatism. Geochim Cosmochim Acta 59:959–977

Pearson DG, Canil D, Shirey SB (2003) Mantle samples included in volcanic rocks: xenoliths and diamonds. In: Carlson RW (ed) Treatise on geochemistry, vol 2. The mantle and core. Elsevier, Amsterdam, pp 171–276

Pisarevsky SA, Natapov LM (2003) Siberia and Rodinia. Tectonophysics 375:221–245

Polyakov AI, Bagdasaryan GP (1986) On the age of young volcanoes in Eastern Siberia and character of compositional evolution of volcanites (in Russian). Geokhimiya No 3:311–317

Press S, Witt G, Seck HA, Ionov DA, Kovalenko VI (1986) Spinel peridotite xenoliths from the Tariat Depression, Mongolia. I: major element chemistry and mineralogy of a primitive mantle xenolith suite. Geochim Cosmochim Acta 50:2587–2599

Rasskazov SV, Boven A, Ivanov AV, Semenova VG (2000) Middle Quaternary volcanic impulse in the Olekma-Stanovoy mobile system: ^{40}Ar–^{39} Ar dating of volcanics from the Tokinsky Stanovik. Tikhookean Geol 19:19–28

Rosen OM, Condie KC, Natapov LM, Nozhkin AD (1994) Archean and Early Proterozoic evolution of the Siberian craton: a preliminary assessment. In: Condie KC (ed) Archean crustal evolution. Elsevier, Amsterdam, pp 411–459

Ross K, Elthon D (1997) Extreme incompatible trace-element depletion of diopside in residual mantle from south of the Kane Fracture Zone. Proc ODP Sci Res 153:277–284

Schmidberger SS, Francis D (1999) Nature of the mantle roots beneath the North American craton: mantle xenolith evidence from Somerset island kimberlites. Lithos 48:195–216

Semenova VG, Solovyeva LV, Vladimirov BM (1984). Deep-seated inclusions in Alkali Basaltoids of the Tokinsky Stanovik (in Russian). Nauka, Novosibirsk, 119 p

Smethurst MA, Khramov AN, Torsvik TH (1998) The Neoproterozoic and Palaeozoic palaeomagnetic data for the Siberian platform: from Rodinia to Pangea. Earth Sci Rev 43:1–24

Smith D (2000) Insights into the evolution of the uppermost continental mantle from xenolith localities on and near the Colorado plateau and regional comparisons. J Geophys Res 105:16769–16781

Sobolev NV (1977) Deep-seated inclusions in kimberlites and the problem of the composition of the upper mantle. Amer Geophys Union, Washington DC, 279 p

Solovyeva LV, Semenova VG, Vladimirov BM, Zavyalova LL, Barankevich VG (1988) Glasses and quenched phases in a spinel lherzolite xenolith from the Tokinsky Stanovik alkalic basaltoids. Trans (Doklady) Acad Sci USSR, Earth Sci Sect 292:106–109

Spetsius ZV, Serenko VP (1990) Composition of the continental upper mantle and lower crust beneath the Siberian platform (in Russian). Nauka, Moscow, 272 p

Streckeisen A (1976) To each plutonic rock its proper name. Earth Sci Rev 12:1–33

Takazawa E, Frey FA, Shimizu N, Obata M (2000) Whole rock compositional variations in an upper mantle peridotite (Horoman, Hokkaido, Japan): are they consistent with a partial melting process? Geochim Cosmochim Acta 64:695–716

Takazawa E, Okayasu T, Satoh K (2003) Geochemistry and origin of the basal lherzolites from the northern Oman ophiolite (northern Fizh block). Geochemistry, Geophysics, Geosystems 4: Paper no 2001GC000232

Ukhanov AB, Ryabchikov ID, Kharkiv AD (1988) Lithospheric mantle of the Yakutian kimberlite province (in Russian). Nauka, Moscow, 286 p

Vannucci R, Bottazzi P, Wulff-Pedersen E, Neumann E-R (1998) Partitioning of REE, Y, Sr, Zr and Ti between clinopyroxene and silicate melts in the mantle under La Palma (Canary Islands): implications for the nature of the metasomatic agents. Earth Planet Sci Lett 158:39–51

Walter MJ (1999) Melting residues of fertile peridotite and the origin of cratonic lithosphere. In: Fei Y, Bertka CM, Mysen BO (eds) Mantle petrology: field observations and high-pressure experimentation. Spec Publ Geochem Soc no 6. Geochemical Society, Houston, pp 225–239

Walter MJ (2003) Melt extraction and compositional variability in mantle lithosphere. In: Carlson RW (ed) Treatise on geochemistry, vol 2. The mantle and core. Elsevier, Amsterdam, pp 363–394

Wiechert U, Ionov DA, Wedepohl KH (1997) Spinel peridotite xenoliths from the Atsagin-Dush volcano, Dariganga lava plateau, Mongolia: a record of partial melting and cryptic metasomatism in the upper mantle. Contrib Mineral Petrol 126:345–364

Xu X, O'Reilly SY, Griffin WL, Zhou X (2003) Enrichment of upper mantle peridotite: petrological, trace element and isotopic evidence in xenoliths from SE China. Chem Geol 198:163–188

Yaxley GM, Kamenetsky V (1999) In situ origin for glass in mantle xenoliths from southeastern Australia: insights from trace element compositions of glasses and metasomatic phases. Earth Planet Sci Lett 172:97–109

Zhang M, Suddaby P, O'Reilly SY, Qiu J (2000) Nature of the lithospheric mantle beneath the eastern part of the Central Asian fold belt: mantle xenolith evidence. Tectonophysics 328:131–156

Zheng J, O'Reilly SY, Griffin WL, Lu F, Zhang M, Pearson NJ (2001) Relict refractory mantle beneath the eastern North China block: significance for lithosphere evolution. Lithos 57:43–66

Zonenshain LP, Kuzmin MI, Natapov LM (1990) Geology of the USSR: a plate tectonic synthesis. Amer Geophys Union, Geodynamics Series 21, Washington DC, 242 p